Received: 4 October 2023 | Revised: 8 March 2024 | Accepted: 24 March 2024

DOI: 10.1002/cne.25611

RESEARCH ARTICLE

JCN RESEARCH IN SYSTEMS NEUROSCIENCE THE JOURNAL OF COMPARATIVE NEUROLOGY WILEY

Parallel executive pallio-motor loops in the pigeon brain

Alina Steinemer | **Annika Simon** | **Onur Güntürkün** | **Noemi Rook**

Department of Biopsychology, Institute of Cognitive Neuroscience, Faculty of Psychology, Ruhr University Bochum, Bochum, Germany

Correspondence
Noemi Rook, Department of Biopsychology, Institute of Cognitive Neuroscience, Faculty of Psychology, Ruhr University Bochum, Universitätsstraße 150, 44801 Bochum, Germany. Email: Noemi.rook@rub.de

Funding information
Deutsche Forschungsgemeinschaft, Grant/Award Numbers: SFB 1280 Project-ID 316803389 subproject A01, SFB1372 Project-ID 395940726 subproject Neu04

Abstract

A core component of the avian pallial cognitive network is the multimodal nidopallium caudolaterale (NCL) that is considered to be analogous to the mammalian prefrontal cortex (PFC). The NCL plays a key role in a multitude of executive tasks such as working memory, decision-making during navigation, and extinction learning in complex learning environments. Like the PFC, the NCL is positioned at the transition from ascending sensory to descending motor systems. For the latter, it sends descending premotor projections to the intermediate arcopallium (AI) and the medial striatum (MSt). To gain detailed insight into the organization of these projections, we conducted several retrograde and anterograde tracing experiments. First, we tested whether NCL neurons projecting to AI (NCL_{arco} neurons) and MSt (NCL_{MSt} neurons) are constituted by a single neuronal population with bifurcating neurons, or whether they form two distinct populations. Here, we found two distinct projection patterns to both target areas that were associated with different morphologies. Second, we revealed a weak topographic projection toward the medial and lateral striatum and a strong topographic projection toward AI with clearly distinguishable sensory termination fields. Third, we investigated the relationship between the descending NCL pathways to the arcopallium with those from the hyperpallium apicale, which harbors a second major descending pathway of the avian pallium. We embed our findings within a system of parallel pallio-motor loops that carry information from separate sensory modalities to

Abbreviations: A, arcopallium; AA, anterior arcopallium; AD, dorsal arcopallium; AFP, anterior forebrain pathway; AI, intermediate arcopallium; AId, dorsal portion of the intermediate arcopallium; AIdm, dorsomedial portion of the intermediate arcopallium; AIvm, ventromedial portion of the intermediate arcopallium; AM, medial arcopallium; Av, ventral arcopallium; Bas, nucleus basalis; BDA, biotinylated dextran amine; CB, calbindin; CR, calretinin; CtB, cholera toxin subunit B; DAB, 3,3-diaminobenzidine; DIP, nucleus dorsointermedius posterior thalami; DLM, medial portion of the dorsolateral thalamic nucleus; DLP, dorsolateral posterior thalamic nucleus; DM, dorsomedial nucleus of the intercollicular complex; DMA, nucleus dorsomedialis anterior thalami; dNCL, nidopallium caudolaterale pars dorsalis; E, entopallium; GP, globus pallidus; HA, hyperpallium apicale; ICo, nucleus intercollicularis; LMAN, lateral magnocellular nucleus of the anterior nidopallium; IMSt, limbic portion of the medial striatum; LSt, lateral striatum; MLd, dorsal nucleus mesencephalicus lateralis; MSt, medial striatum; NCC, nidopallium caudocentrale; NCL, nidopallium caudolaterale; NCLd, nidopallium caudolaterale pars dorsale; NCLl, nidopallium caudolaterale pars lateralis; NCLm, nidopallium caudolaterale pars mediale; NCM, caudomedial nidopallium; Nd, nidopallium dorsale; NFT, nidopallium frontotrigeminale; NI, nidopallium intermedium; NIL, nidopallium intermedium pars laterale; NIM, nidopallium intermedium medialis; NIML, nidopallium intermedium medialis pars laterale; nXIIts, hypoglossal nucleus, tracheosyringeal portion; OM, tractus occipitomesencephalicus; Ov, nucleus ovoidalis; PBST, phosphate-buffered saline with Triton X-100; PFA, paraformaldehyde; PFC, prefrontal cortex; PMP, posterior motor pathway; PoA, nucleus posterioris amygdalopallii; PrV, principal sensory trigeminal brainstem nucleus; PrVd, dorsal portion of the sensory trigeminal brainstem nucleus; PrVv, ventral portion of the sensory trigeminal brainstem nucleus; PV, parvalbumin; RA, robust nucleus of the arcopallium; Rt, nucleus rotundus; sLSt, somatic portion of the lateral striatum; sMSt, somatic portion of the medial striatum; SN, substantia nigra; SNc, substantia nigra pars compacta; SNr, substantia nigra pars reticulata; St, striatum; TeO, tectum opticum; TnA, nucleus taeniae amygdalae; TSM, tractus septo-mesencephalicus; VIA, thalamic ventrointermediate area; VP, ventral pallidum; VTA, ventral tegmental area.

Alina Steinemer and Annika Simon contributed equally to this study.

Onur Güntürkün and Noemi Rook contributed equally to this study.

different subpallial systems. Our results also provide insights into the evolution of the avian motor system from which, possibly, the song system has emerged.

1 | INTRODUCTION

Birds like pigeons are capable of a variety of higher cognitive functions (Güntürkün et al., 2017), such as orthographic processing (Scarf et al., 2016), object permanence (Dumas & Wilkie, 1995), and numerical competence (Scarf et al., 2011). They also excel in navigating across hundreds of kilometers (Prior et al., 2004) and quickly learn all kinds of complex learning tasks such as categorization (Anderson et al., 2020; Pusch et al., 2023) and serial extinction (Packheiser et al., 2021). Strikingly, some corvid species are even on par with primates in a broad variety of cognitive domains (Balakhonov & Rose, 2017; Clayton & Emery, 2015; Güntürkün & Bugnyar, 2016; Pika et al., 2020). This is particularly noteworthy, as avian and mammalian brains are differently organized despite similarities on the overall connectional (Shanahan et al., 2013) and microcircuit level (Ahumada-Galleguillos et al., 2015; Fernández et al., 2021; Mouritsen et al., 2016; Stacho et al., 2020; Wang et al., 2010). In birds, a core neural component for these higher cognitive functions is the nidopallium caudolaterale (NCL) (Ditz & Nieder, 2015; Güntürkün, 1997; Hahn et al., 2021; Lengersdorf et al., 2014; Packheiser et al., 2021), an integration center that receives multimodal sensory input from auditory, visual, and trigeminal systems (Herold et al., 2011; Kröner & Güntürkün, 1999; Leutgeb et al., 1996) and is considered analogous to the mammalian prefrontal cortex (PFC) (Güntürkün, 2005, 2012; Güntürkün et al., 2021). Although the NCL varies in size, position, and complexity, depending on the species' ecological needs (Eugen et al., 2020; Kobylkov et al., 2022; Ströckens et al., 2022), an outstanding common characteristic is its massive dopaminergic innervation originating in the ventral tegmental area (VTA) and substantia nigra (SN) (Eugen et al., 2020; Kobylkov et al., 2022; Waldmann & Güntürkün, 1993). Moreover, the avian NCL harbors two main descending projections, one to the striatum akin to frontostriatal circuits and one to the premotor arcopallium (Herold et al., 2011; Kröner & Güntürkün, 1999).

The arcopallium receives inputs mainly via the tractus dorsoarcopallialis and the tractus fronto-arcopallialis (Zeier & Karten, 1971) that originate from the multisensory NCL and from somatosensory, visual, and trigeminal areas. It is a highly heterogeneous area encompassing a multitude of subnuclei (medial arcopallium [AM], intermediate arcopallium [AI], anterior arcopallium [AA], dorsal arcopallium [AD]), of which AI and AA have premotor functions (Herold et al., 2018; Zeier & Karten, 1971). Both subunits are homotopically and reciprocally connected via the anterior commissura (Letzner et al., 2016) and form the origin of the tractus occipitomesencephalicus (OM), which is a massive fiber bundle that descends to the diencephalon, mesencephalon, and brainstem (Fernández, Morales, et al., 2020). These premotor subnuclei resemble the mammalian premotor cortex in function (Gao et al., 2018; Zemel et al., 2022), connectivity (Butler et al., 2011; Kuenzel et al., 2011), and neurochemistry (Herold et al., 2018; Mello et al., 2019). They seem to be relay structures that link the executive control of the NCL to brainstem motor areas that guide actions within the audiomotor domain (Wild et al., 1993) and the visuomotor domain (Cohen et al., 1998; Rook et al., 2020; Xiao & Güntürkün, 2018). Amygdala subnuclei beneath the arcopallium (nucleus posterioris amygdalopallii [PoA] and nucleus taeniae amygdalae [TnA]) serve limbic functions and resemble the mammalian amygdala (Fujita et al., 2020; Shanahan et al., 2013; Yamamoto & Reiner, 2005; Yamamoto et al., 2005; Zeier & Karten, 1971). Because of their anatomical linkage, the region is generally referred to as arcopallium/amygdala complex (Herold et al., 2018).

The avian striatum is considered homologous to the mammalian striatum, based on shared cellular and anatomical characteristics (Kuenzel et al., 2011; Medina et al., 2014; Reiner, 2002; Reiner et al., 2004), and functional studies have shown its involvement in learning and action selection (Rose et al., 2013; Watanabe, 2001; Xiao et al., 2018, 2021; Yin, 2010). The striatum receives afferents from many different regions of the pallium including the NCL and the nidopallium intermedium medialis pars laterale (NIML), which are both higher associative areas (Kröner & Güntürkün, 1999; Veenman et al., 1995). From the striatum, information is further relayed via the globus pallidus (GP) and substantia nigra pars reticulata (SNr) to the thalamus (Jiao et al., 2000). Finally, the thalamus projects back to the NCL and NIML (Kitt & Brauth, 1982; Kröner & Güntürkün, 1999). Overall, this circuit resembles cortico-striato-thalamo-cortical loops in mammals. In both mammals and birds, these connections are involved in processing sequential action patterns (Hahn & Rose, 2023; Helduser & Güntürkün, 2012; Rook, Tuff, Packheiser, et al., 2021; Xiao & Roberts, 2021; Yin, 2010).

Here, we set out to comprehensively study the connectional architecture of this system and to embed our findings into the overall network of avian pallio-motor loops. In songbirds, specialized projections to the arcopallium and striatum exist as part of the song system underlying vocal learning (Brenowitz et al., 1997; Jarvis et al., 2000; Nottebohm, 2005). Here, distinct song nuclei form an anterior forebrain pathway (AFP) that is involved in sensorimotor song acquisition and adult song plasticity, and a posterior motor pathway (PMP) that is involved in the motor aspect of song production (Bolhuis et al., 2010; Farries, 2004; Moorman et al., 2011). The song nucleus HVC (acronym used as proper name), which is located within the NCL (Matsunaga et al., 2008), is of particular interest as it feeds information into both pathways. On the one hand, it sends projections to Area X within the striatum (AFP), and on the other hand, it sends projections to the robust nucleus (RA) within the arcopallium (PMP) (Düring et al., 2020; Trusel et al., 2022) (Figure 1).

Neurons within HVC belong to one of three classes: interneurons, neurons projecting to Area X (HVC_X neurons), or neurons projecting to

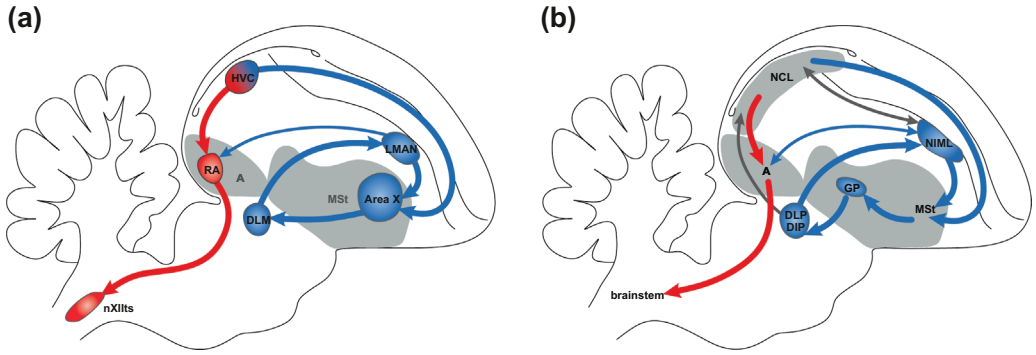

FIGURE 1 Comparison between the connectivity of the oscine song nuclei and comparable areas in the pigeon brain. (a) Schematic illustration of the oscine song system. The anterior forebrain pathway (AFP) is depicted in blue, and the posterior motor pathway (PMP) is depicted in red. (b) Pathways that resemble the song system in its connectivity in the pigeon brain. For abbreviations, see list.

RA (HVC_{RA} neurons), each exhibiting characteristic functional properties (Daou et al., 2013; Mooney, 2000). These differences in function come along with distinct morphological features. It has been reported that HVC_X neurons display greater soma sizes (Mooney, 2000; Paton et al., 1985) as well as different dendritic profiles (Benezra et al., 2018) compared to HVC_{RA} neurons. As Area X is part of the AFP and RA is part of the PMP, HVC projections toward the two main song pathways are already separated at the cellular level. It is conceivable that this target-specific specialization of HVC neurons is an evolutionary consequence of vocal learning and might not exist in nonvocal learning species. Within the avian class, vocal learning is only found in three groups: songbirds (Passeriformes), hummingbirds (Trochiliformes), and parrots (Psittaciformes) (Gahr, 2000; Jarvis & Mello, 2000). These three orders show a remarkably similar neural organization for their song systems, although they are only distantly related (Hackett et al., 2008; Jarvis et al., 2015). One prominent evolutionary theory, the motor theory of vocal learning, suggests that the three avian vocal learning systems evolved independently as specializations from a pre-existing movement control system inherited from a common ancestor (Feenders et al., 2008). Indeed, the authors found that in both vocal learners and nonlearners, body movements activate the same brain areas; in vocal learners, these brain areas are adjacent to their song nuclei.

In nonvocal learning pigeons, however, it is not yet known whether NCL projection neurons are segregated in a way that is similar to HVC neurons in songbirds. In this respect, it is conceivable that pigeons represent an ancient neural system for descending premotor pathways that served as the basis for the derived and elaborated song system. This ancient system could guide response selection with a uniform neuronal population with bifurcation axons controlling both arcopallial and striatal motor output systems. The current study aims at unravelling the organization of the descending premotor projections from the pigeon NCL. Therefore, we want to answer the following overlapping questions: First, are the arcopallial and striatal projections of the NCL constituted by a single neuronal population with bifurcating axons or do they consist of two divergent populations as found in oscines (Wild et al., 2005)? Second, in case of two divergent neuronal populations, do pigeon NCL projection neurons differ in the sizes of their somata as reported for HVC projection neurons (Mooney, 2000; Wild et al., 2005)? Third, can we reveal a topographic organization of the striatal NCL projections similar to the reported topography of the arcopallial NCL projections (Fernández, Morales, et al., 2020)? Fourth, how are these descending pathways from NCL and arcopallium related to the hyperpallium apicale (HA), from which the second major descending pathway of the avian pallium emerges? Building on previous studies (Fernández, Morales, et al., 2020; Kröner & Güntürkün, 1999; Veenman et al., 1995; Wild et al., 1985), we thus aim to shed light onto these questions by conducting anterograde and retrograde tracing experiments in pigeons and examining expression patterns of different calcium-binding proteins. Ultimately, we embed our discussion into the evolution of the avian pallio-motor system, from which possibly the song system has emerged.

2 | METHODS

2.1 | Subjects

Twenty-six pigeons (*Columba livia*) of both sexes that were obtained from local breeders were used in this study. Pigeons were housed in individual cages with a 12-h dark/light cycle and had ad libitum access to food and water. All surgical procedures were performed according to the principles regarding the care and use of animals adopted by the German Animal Welfare Law for the prevention of cruelty to animals in agreement with the Directive 2010/63/EU of the European Parliament of the Council of September 22, 2010 and were approved by the animal ethics committee of the Landesamt für Natur, Umwelt und Verbraucherschutz (LANUV) NRW, Germany. All efforts were made to minimize the number of subjects and their suffering.

2.2 | Surgical procedure and tracer injections

Animals were anesthetized by an intramuscular injection containing a 7:3 mixture of ketamine (Ketavet 100 mg/mL; Zoetis GmbH) and xylazine (Rompun 20 mg/mL; Bayer Vital GmbH). Injections were

administered into both breast muscles using 0.15 mL for each 100 g bodyweight. This corresponds to 105 mg ketamine and 9 mg xylazine per kilogram bodyweight. Prior to the surgical procedure, feathers on top of the head and covering the ears were cut. Once the pigeons showed no longer any pain reflexes, they were positioned in a stereotactic apparatus. For arcopallial and striatal injections, a modified stereotactic device was used, allowing for a rotation of the head along the longitudinal axis through 90° to the left and right. At first, 10 mg lidocaine (Xylocain; Aspen Pharma Trading Limited) was applied to the scalp for topical anesthesia. Then, the scalp was incised to expose the cranial bone. The skull was opened with a dental drill, and a glass micropipette (inner tip diameter 10–20 mm) mounted to a mechanical pressure device (WPI Nanoliterinjector; World Precision Instruments) was lowered into the different target structures according to the stereotactic coordinates of the pigeon brain atlas (Karten & Hodos, 1967). All tracers were injected in 2-nL or 9.2-nL steps with 10 s in between each step. When one injection was completed, the micropipette was drawn back after a dwelling time of 5 min. Injected volumes ranged between 30 and 350 nL, according to the size of the targeted structure. Each animal received tracer injections of cholera toxin subunit B (CtB; Sigma), biotinylated dextran amine (BDA; molecular weight 3000; Thermo Fisher Scientific), or a combination of both into the medial striatum (MSt), AI, HA, or NCL. Both CtB (1% in deionized water) and BDA 3000 (10% in 3% dimethyl sulfoxide or 10% in phosphate buffered saline; [PBS]) were used as retrograde tracers. However, we also analyzed anterogradely labeled fibers after CtB injections.

2.3 | Perfusion and tissue processing

After a survival time of 2 (CtB injections) or 7 days (BDA injections), the animals were deeply anesthetized with equithesin (10 mg pentobarbital/mL, 0.45 mL/100 g bodyweight) and transcardially perfused with 0.9% sodium chloride (NaCl) followed by cold (4°C) 4% paraformaldehyde (PFA) in phosphate buffer (PB; 0.12 M, pH 7.4). Brains were removed from the skull and postfixated in 4% PFA with 30% sucrose at 4°C for 2 h. For subsequent cryoprotection, they were immersed in PBS with 30% sucrose for at least 24 h. To facilitate slicing, brains were embedded in 15% gelatin/30% sucrose in PBS. Gelatin blocks were then fixated in 4% PFA in PBS for 24 h and, after that, cryoprotected in PBS with 30% sucrose for at least 24 h. All brains were cut in frontal plane in 30-μm or 40-μm-thick slices using a freezing microtome (Leica, Wetzlar, Germany). Slices were collected in 10 series and stored in PBS containing 0.1% sodium azide at 4°C until further processing.

2.4 | Immunohistochemistry

For all immunohistochemical staining procedures, every 10th slice of each brain was used. Tracers were visualized with a DAB (3,3-diaminobenzidine) staining procedure in free-floating slices. When only one tracer was injected, we followed our regular staining protocols as described in the following. For staining of BDA, slices were first rinsed in PBS (3 × 10 min). Then, they were incubated in 0.3% hydrogen peroxide (H_2O_2) in distilled water for 30 min to block endogenous peroxidases. After that, slices were rinsed again (3 × 10 min in PBS) and transferred into an avidin–biotin–peroxidase solution (Vector Laboratories-Vectastain Elite ABC kit; 1:100 in PBS containing 0.3% Triton-X-100 [PBST]) for 60 min. After further rinsing (3 × 10 min in PBS and 1 × 5 min in 0.1 M sodium acetate buffer, pH 6.0), slices were incubated in DAB solution, which was composed of DAB (0.2 mg/mL), ammonium nickel sulfate (25 mg/mL), cobalt chloride (0.4 mg/mL), ammonium chloride (0.4 mg/mL), and β-D-glucose (4 mg/mL) in 0.1 M sodium acetate buffer (pH 6.0). The reaction was initiated by adding glucose oxidase (80—100 μL/50 mL DAB solution), which led to the oxidation of β-D-glucose. During the reaction, staining intensity was visually controlled permanently, and the solution was changed every 10 min. The staining reaction was stopped after 30 min by rinsing the slices in 0.1 M sodium acetate buffer (3 × 5 min) and PBS (3 × 5 min). For staining of CtB, slices were first rinsed (3 × 10 min in PBS). Then, they were incubated in 0.3% H_2O_2 in distilled water for 30 min and rinsed (3 × 10 min in PBS). After that, they were transferred into 10% normal rabbit serum (Vector Laboratories-Vectastain Elite ABC kit) in PBST for 60 min to block unspecific binding sites. Subsequently, slices were incubated in the primary antibody solution containing a goat anti-CtB antibody (1:5000 in PBST; RRID: AB_211712; Calbiochem) overnight at 4°C. Following further rinsing (3 × 10 min in PBS), slices were incubated in the biotinylated secondary anti-goat antibody (1:500 in PBST; Vector Laboratories-Vectastain Elite ABC kit) for 60 min at room temperature. Following this, slices were rinsed in PBS (3 x 10 min) and incubated in an avidin–biotin–peroxidase solution (Vector Laboratories-Vectastain Elite ABC kit; 1:100 in PBST for 60 min. Thereafter, slices were again rinsed (3 × 10 min in PBS and 1 × 5 min in 0.1 M sodium acetate buffer, pH 6.0) and the DAB staining reaction was carried out as described above. When BDA and CtB were injected into the same brain, we stained the two tracers in a sequential fashion with BDA first and CtB second. In order to be able to differentiate the two tracers within the same slice, we slightly adapted the staining protocols. For the BDA staining, the DAB reaction was modified by omitting the addition of ammonium nickel sulfate to the DAB solution, resulting in a brown reaction product. For the CtB staining, the protocol remained unchanged, with the use of ammonium nickel sulfate resulting in a black reaction product. As a last step, all slices were mounted onto gelatin-coated slides and dehydrated in ethanol and xylene, and coverslipped with DPX (Fluka, Munich, Germany).

For fluorescence stainings, only slices including the NCL were selected. In addition to retrogradely BDA-labeled neurons, we visualized the calcium-binding proteins calbindin (CB), parvalbumin (PV), and calretinin (CR). Slices were first rinsed (3 × 10 min in PBS) and then incubated in a combination of 5% normal horse serum (Vector Laboratories-Vectastain Elite ABC kit) and 5% normal goat serum (Vector Laboratories-Vectastain Elite ABC kit) in PBST for 30 min at room temperature to block unspecific binding sites. Without rinsing, slices were then incubated in either a polyclonal rabbit anti-CB antibody (RRID:AB_10000340; Swant), guinea pig anti-PV

antibody (RRID:AB_2665495; Swant), or guinea pig anti-CR antibody (RRID:AB_10000342; Swant) 1:1000 in PBST with 5% bovine serum albumin at 4°C. Seventy-two hours later, slices were rinsed (3 × 10 min in PBS) and then incubated in a combination of streptavidin AlexaFluor594 conjugate (Invitrogen, Darmstadt, Germany) with either a goat anti-rabbit AlexaFluor488 antibody (Invitrogen, Darmstadt, Germany) or a donkey anti-guinea pig AlexaFluor488 antibody (Jackson ImmunoResearch, Pennsylvania, USA). Both the secondary antibody and streptavidin were incubated 1:500 in PBST for 90 min at room temperature. After final rinsing (3 × 10 min in PBS), slices were mounted onto glass slides (Superfrost Plus; Thermo Scientific) and embedded with Fluoromount-G (SouthernBiotech, Birmingham, USA). We ensured that exposure to light was reduced to a minimum in order to preserve as much fluorescence as possible.

2.5 | Microscopic analysis

All slices comprising the respective structures of interest of one brain series (every 10th slice) were analyzed. For imaging DAB stainings, we used a ZEISS Axio Imager.M1 with mounted cameras (AxioCam MRm ZEISS 60N-C 2/3″ 0.63× for monochrome images and AxioCam 506 ZEISS 60N-C 1″ 1.0× for color images) at 100×, 200×, or 400× magnification. For imaging fluorescence staining, we used a ZEISS Axio Scan.Z1 at 100× magnification. Measurement of cell sizes of NCL projection neurons was conducted by using the Image Analysis module implemented in ZEN 3.8 Pro. Upper and lower thresholds for automatic segmentation of cells were determined with Otsu method for all individual images. Further parameters for segmentation were set to (smooth: none; sharpen: none; minimum area: 25 pixels; separate: morphology; count: 6; roundness: >0.2). After automatic segmentation was completed, selected cells were visually double checked. Outliers were determined for cell diameter and cell area and defined as observations that fall below Q1−1.5 IQR or above Q3+1.5 IQR and excluded from the data set. After that, multiple linear regression was used to test if "brain area" predicted "cell area" and "cell diameter" after correcting for subject and interaction effects.

3 | RESULTS

3.1 | Double tracer injections into the striatum and arcopallium

To identify potential biprojecting NCL neurons, which target both the MSt and the arcopallium, two different retrograde tracers were injected into the same hemisphere, CtB and BDA. The pigeon striatum consists of a medial and a lateral (LSt) part and extends in the anteroposterior direction from A6.50 to A13.00 (Figure 2a,c,d). The arcopallium comprises several substructures—an anterior (AA), a dorsal (AD), an intermediate (AI), and a medial part (AM)—and extends from A4.50 to A8.00 (Figure 2b,d) (Herold et al., 2018). The NCL extends from A4.00 to A7.50 (Figure 2b–d) and does not comprise further substructures based on its cytoarchitecture, albeit Kröner and Güntürkün (1999) and Herold et al. (2011) proposed a medial/lateral division of the NCL based on its connectivity and receptor distribution (Figure 2e). All stereotactic coordinates were obtained from the pigeon brain atlas (Karten & Hodos, 1967).

For this experiment, eight pigeons received double tracer injections into one or both hemispheres. CtB injections were placed at A10.00 for MSt (Figure 3a,b), and BDA injections were placed at A6.50 for AI (Figure 3a,c). The spread of CtB was restricted to the striatum extending from A10.50 to A9.50, including MSt, LSt, and GP. The spread of BDA was restricted to the arcopallium up to A7.00. The distribution of CtB- and BDA-labeled neurons within the NCL is schematically shown in Figure 3a. Numerous CtB- and BDA-labeled neurons were detected throughout the entire NCL. After striatal injections, labeled NCL neurons reached from A5.00 to A7.50. Especially toward caudal parts, cells clustered predominantly in the ventral and ventromedial NCL, whereas they shifted more laterally toward the ventricle in NCLl in the rostral part (A6.50 to A7.50). The highest density of CtB-labeled cells was detected at A6.50 and the lowest at A5.00. After arcopallial injections, labeled NCL neurons were found in a range from A5.00 to A7.00. In the caudal part (A5.00 to A6.00), labeled neurons were distributed in dorsal NCL and traversed closer to the ventricle in NCLl toward rostral sections (A6.50 to A7.00). The highest density of BDA-labeled cells was detected at A6.00, and only a small number of cells were found at A7.00. Comparing labeled neurons of both injections, no double-labeled and thus no biprojecting cells were detected. Instead, a differentiated projection pattern became evident. Neurons within the dorsal NCLl projected predominantly to the arcopallium, whereas neurons in central NCL and NCLm targeted the striatum, with only a small area of overlap at A6.50 (Figure 3a,d–f).

3.2 | Striatum tracer injections

To map the topographic NCL projection pattern toward the arcopallium in greater detail and to investigate a putative topography of striatal NCL projections, several CtB injections into either the striatum, the arcopallium, or the NCL were conducted. For retrograde tracing of striatal connections, eight birds received injections into MSt along the anteroposterior axis at either A11.50, A10.50, or A9.50. We mainly searched for labeled neurons within NCL and arcopallium, but we also included the HA, as it is known to be the only second pallial structure of the avian telencephalon with descending motor projection to both the striatum and brainstem (Shimizu et al., 1995; Wild & Williams, 2000). Furthermore, we included the anterior nidopallium (especially NIML) into the analysis as it has been compared to the pallial area LMAN of the AFP in songbirds that shows strong connections with parts of the striatum, arcopallium, and NCL (Figure 1b). Injection sites and the distribution of labeled neurons are schematically illustrated in Figure 4. In the following, we describe one individual case for each targeted AP coordinate within MSt.

In case 962, the CtB injection was administered into MSt at A11.50 (Figure 4, green panel, and Figure 5a). Tracer diffusion ranged from

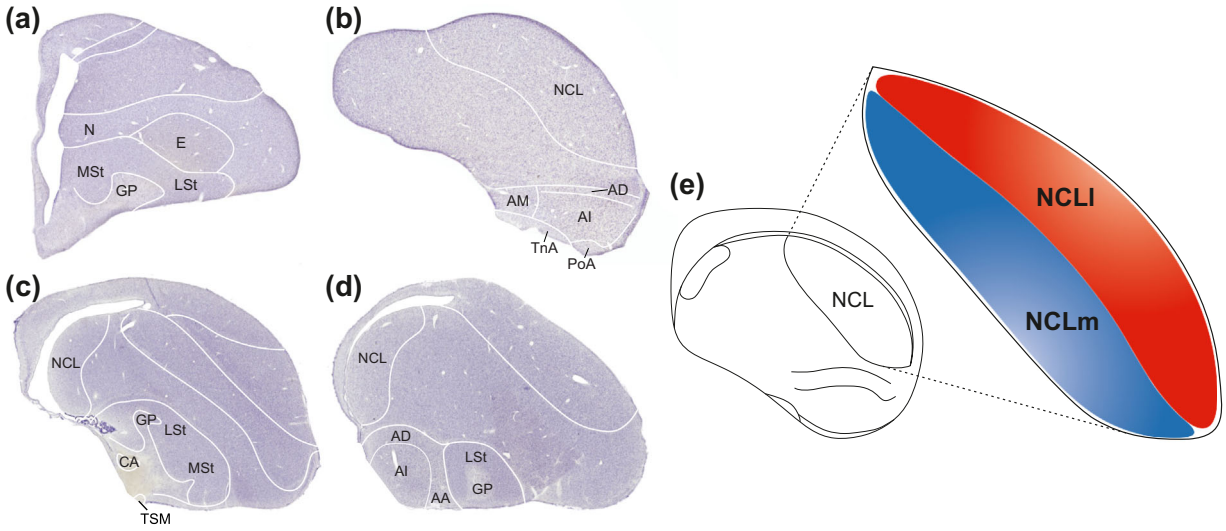

FIGURE 2 Locations of striatum, arcopallium, and nidopallium caudolaterale in the pigeon brain in a cresyl violet staining. (a) Frontal section at A10.00. (b) Frontal section at A6.00. (c) Sagittal section at L6.50. (d) Sagittal section at L2.50. (e) Nomenclature of NCL subdivisions used in this study. We defined a medial/lateral division that follows the curvature of the NCL. For abbreviations, see list.

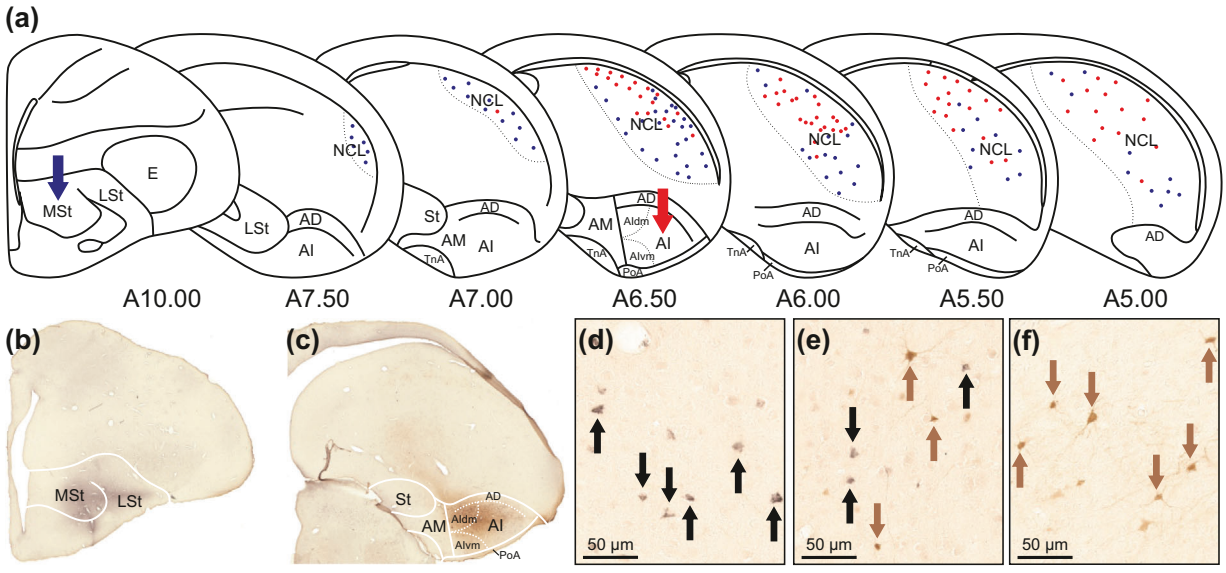

FIGURE 3 Double retrograde tracing of striatal and arcopallial projections of the pigeon NCL. (a) Schematic illustration of the rostrocaudal extent of retrogradely labeled neurons within NCL following injections of CtB into MSt and BDA into AI. A blue and a red arrow mark the cores of the striatal and arcopallial injections, respectively. Blue dots represent retrogradely labeled CtB neurons, and red dots represent retrogradely labeled BDA neurons. Black arrows indicate retrogradely labeled neurons within NCL after MSt injection, and brown arrows indicate retrogradely labeled neurons within NCL after AI injection. (b) Injection site of CtB into the striatum. (c) Injection site of BDA into the arcopallium. (d) CtB labeling in the ventromedial NCL. (e) CtB (black) and BDA (brown) labeled neurons in the overlapping area. (f) BDA-labeled neurons in the dorsolateral NCL. For abbreviations, see list.

A11.00 to A11.75, including LSt. Retrogradely labeled neurons were found within NIML (Figure 5d), NCL (Figure 5g), AA, AD, and AI (Figure 5j), and HA (Figure 4). Within HA, labeled neurons ranged from A10.50 to A11.50. Within the arcopallium, labeled neurons ranged from A6.50 to A7.75 and were predominantly located in the lateral third of AI and AD. Visual inspections revealed that AI neurons exhibited larger soma sizes than AD neurons. Within the anterior nidopallium, some retrogradely labeled cells were found in the anterior sections of NIML between A10.50 and A11.50 directly dorsal to the injection site within MSt. Within NCL, labeled neurons ranged from A5.50 to A7.50 and were predominantly located in the ventral portion.

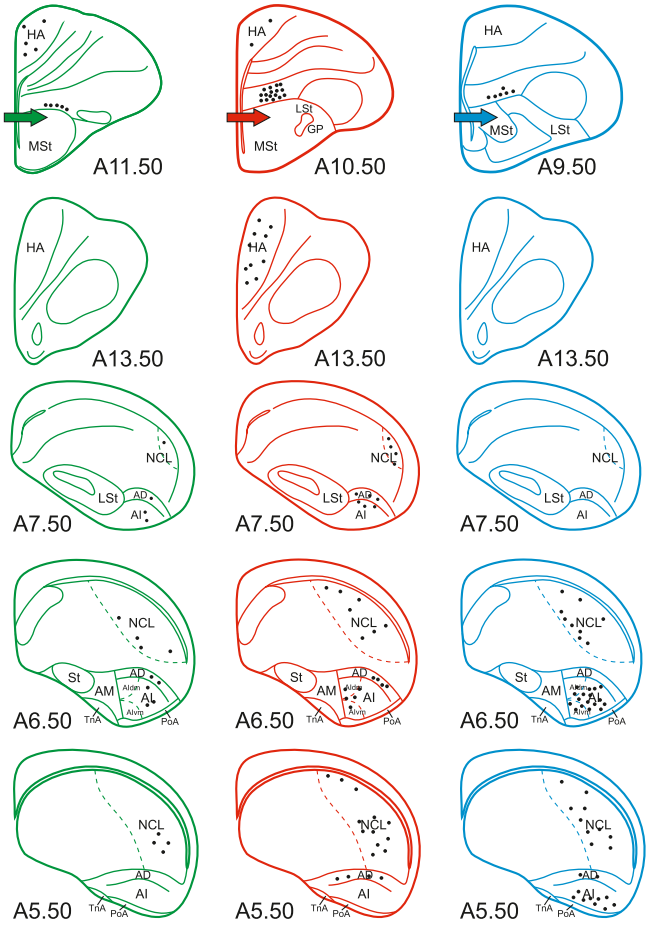

FIGURE 4 Schematic illustration of striatal injection sites and the rostrocaudal extent of retrogradely labeled neurons within the NCL, arcopallium, and anterior nidopallium. The core of the striatal injection site is marked by an arrow. Dots represent retrogradely labeled neurons. Each animal is allocated a different color for better illustration. Case 962 is illustrated in green (left panel; CtB injection at A11.50), case 837 is illustrated in red (middle panel; CtB injection at A10.50), and case 699 is illustrated in blue (right panel; CtB injection at A9.50). For abbreviations, see list.

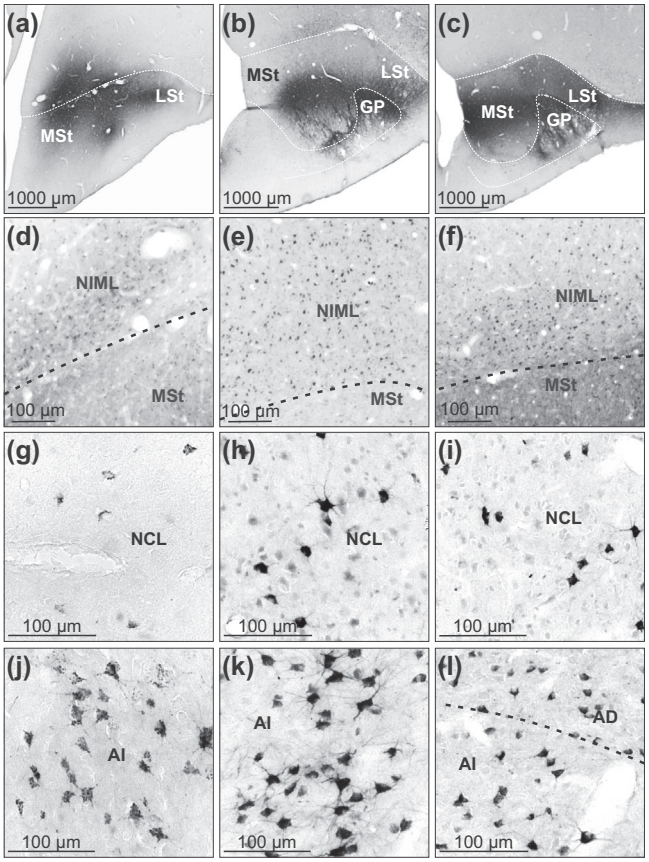

FIGURE 5 Striatal injection sites and retrogradely labeled neurons within NIML, NCL, and arcopallium. (a) CtB injection site at A11.50 (case 962). (b) CtB injection site at A10.50 (case 837). (c) Injection site at A9.50 (case 699). (d–f) Retrogradely labeled neurons within NIML following injections of CtB at A11.50 (d), A10.50 (e), and A9.50 (f). (g–i) Retrogradely labeled neurons within ventrocentral NCL following injections at A11.50 (g), A10.50 (h), and A9.50 (i). (j–l) Retrogradely labeled neurons within AI following injections of CtB at A11.50 (j), A10.50 (k), and A9.50 (l). For abbreviations, see list.

In case 837, CtB was injected into MSt at A10.50 (Figure 4, red panel, and Figure 5b). Tracer diffusion ranged from A10.50 to A11.00. Retrogradely labeled neurons were found within NIML (Figure 5e), NCL (Figure 5h), AD and AI (Figure 5k), and HA (Figure 4). Within HA, labeled neurons were detected in a range from A9.00 to A13.50 with a higher number in the anterior portion (A11.00 to A13.50). Labeled neurons within AI were detected between A6.00 and A7.50 and were predominantly located in the dorsomedial (AIdm) and ventromedial (AIvm) part but shifted more laterally toward the rostral portion. Within the anterior nidopallium, a large number of retrogradely labeled cells were found in NIML between A9.50 and A11.50 directly dorsal to the injection site within MSt. Within NCL, labeled neurons ranged from A5.50 to 7.50. At A5.50, neurons were mainly located in the ventral portion, but some cells were also located in the dorsal NCLl. More rostrally at A6.50, neurons were mainly located in the dorsal NCL.

In case 699, the CtB injection was administered into MSt at A9.50 (Figure 4, blue panel, and Figure 5c). Tracer diffusion ranged from A9.00 to A10.00. The injection resulted in labeled neurons within NIML (Figure 5f), NCL (Figure 5i), and AI and AD (Figure 5l). In contrast to the other cases, no labeled neurons were detected within HA. Concerning the arcopallium, neurons were found in a range between A5.50 and A7.00, encompassing the entire AI and most of AD. A small band of retrogradely labeled neurons was found in the ventral portions of NIML between A9.50 and A11.50 directly dorsal to the injection site within MSt. The pattern of NCL projection neurons was similar to case 837, with most neurons being located in the ventral portion and a smaller number being located in the dorsal NCLl.

Moreover, injections into MSt (Figure 6a) also labeled neurons and fibers within the VTA, substantia nigra pars compacta, and the dorsal thalamus (nucleus dorsomedialis anterior thalami [DMA] and the medial portion of the dorsolateral thalamic nucleus [DLM]) (Figure 6b,e–h). Moreover, we found labeled fibers within the ventral pallidum (VP) (Figure 6c,d).

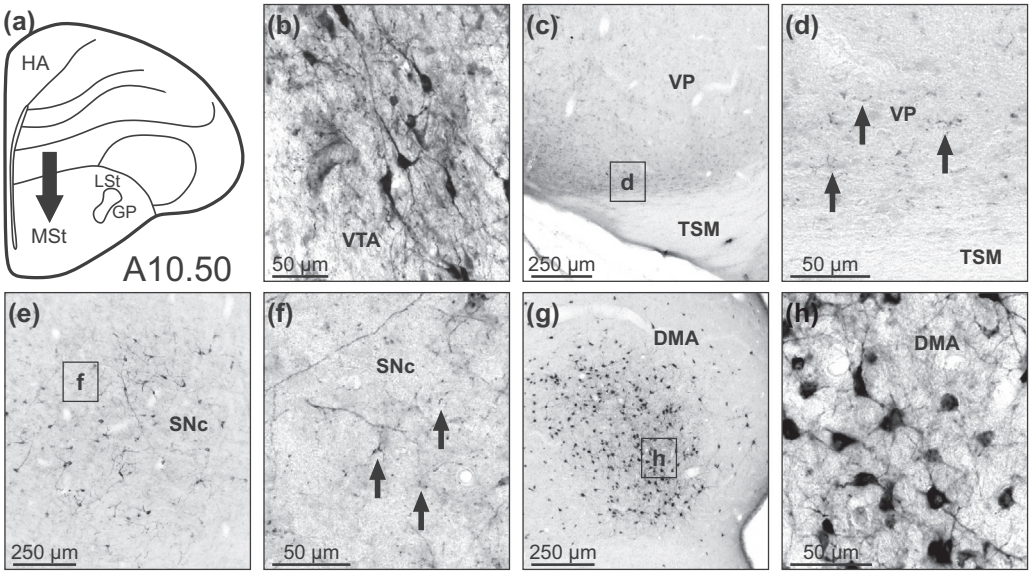

FIGURE 6 Retrogradely labeled neurons and anterogradely labeled fibers in brainstem, subpallial, and thalamic structures following a CtB injection into the medial striatum. (a) Schematic illustration of the CtB injection site at A10.50. (b) Labeled neurons and fibers within VTA. (c) Labeled fibers within VP. (d) Enlargement of the box depicted in panel (c). Black arrows indicate labeled fibers within VP. (e) Labeled neurons and fibers within SNc. (f) Enlargement of the box depicted in panel (e). Black arrows indicate labeled fibers within SNc. (g) Labeled neurons and fibers within DMA. (h) Enlargement of the box depicted in panel (g). For abbreviations, see list.

Taken together, retrogradely labeled neurons within NCL were detected after all injections, but with the highest number after injections into the caudal MSt. Retrograde labeling within NIML was also always observable but most extensively for injections into the mid MSt. Labeled neurons within HA were detected after injections into the rostral MSt only. Numerous labeled neurons within AI were detected after injections into the caudal MSt, but only few neurons after injections into the more rostral portions. Moreover, few neurons within AD were detected after all injections, with a slightly higher number after injections into the mid MSt. Additionally, retrogradely labeled neurons and anterogradely labeled fibers were found within the brainstem, subpallial, and thalamic structures.

3.3 | Arcopallium tracer injections

For retrograde tracing of arcopallial connections, six birds received CtB injections into AI along the anteroposterior axis at either A7.50, A6.50, or A5.50. Two of these birds also received an injection into contralateral MSt and were therefore also included in the striatal tracing described above. We searched for labeled neurons within NCL and HA. Injection sites and the distribution of labeled neurons are schematically illustrated in Figure 7. In the following, we describe one individual case for each targeted AP coordinate within AI.

In case 937, CtB was injected into the AI at A7.50 (Figure 7, green panel, and Figure 8a) leading to retrogradely labeled neurons within NCL (Figure 8d) and within HA at A11.50. Within NCL, they ranged from A5.00 to A6.50 and were located along the ventricle in NCLl. In case 458, the CtB injection was administered into the AI at A6.50 (Figure 7, red panel, and Figure 8b), resulting in a similar pattern of

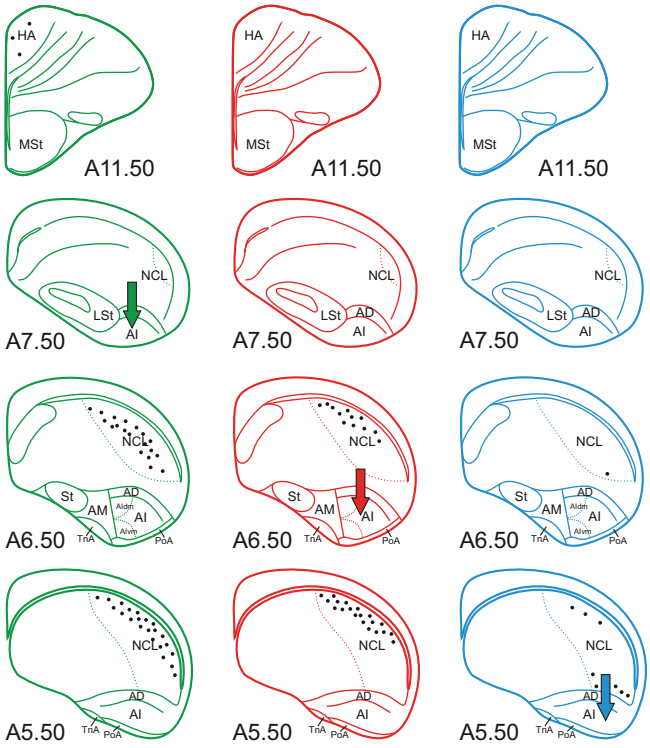

FIGURE 7 Schematic illustration of arcopallial injection sites and the rostrocaudal extent of retrogradely labeled neurons. The core of the arcopallial injection site is marked by an arrow. Dots represent retrogradely labeled neurons. Each animal is allocated a different color for better illustration. Case 937 is illustrated in green (left panel; CtB injection at A7.50), case 458 is illustrated in red (middle panel; CtB injection at A6.50), and case 903 is illustrated in blue (right panel; CtB injection at A5.50). For abbreviations, see list.

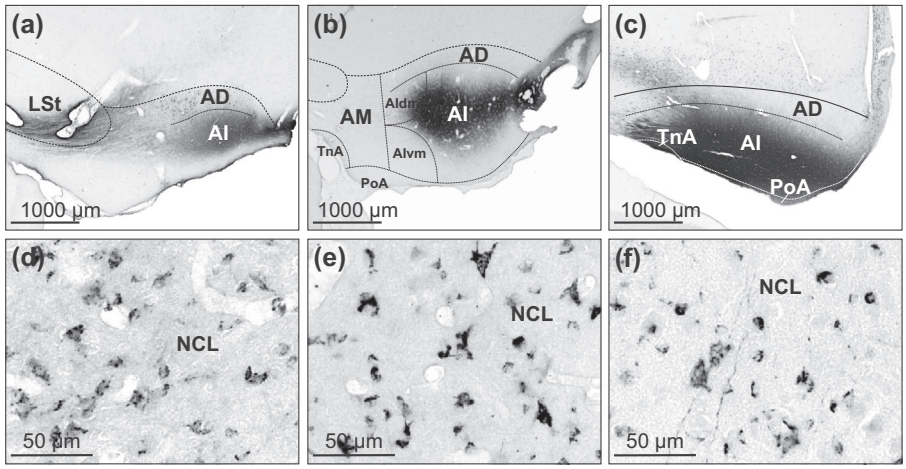

FIGURE 8 Arcopallial injection sites and retrogradely labeled neurons within NCL. (a) CtB injection site at A7.50 (case 937). (b) Injection site at A6.50 (case 458). (c) Injection site at A5.50 (case 903). (d–e) Retrogradely labeled neurons within lateral NCL following injections at A7.50 (d) and A6.50 (e). (f) Retrogradely labeled neurons within ventral NCL following an injection at A5.50. For abbreviations, see list.

labeled neurons within the NCL (Figure 8e). In contrast to case 937, no neurons were found in HA. In case 903, CtB was injected into the AI at A5.50 (Figure 7, blue panel, and Figure 8c), but the tracer spread also included the TnA and PoA. Labeled neurons were solely detected within the NCL (Figure 8f), ranging from A6.50 to A5.50. Neurons were predominantly located within the ventral portion close to the arcopallium. Only a few neurons were detected in the dorsal NCLl.

Taken together, we found labeled neurons within HA after injection into rostral AI only. Apart from this finding, all detected neurons were confined to the NCL. Labeled neurons after injections into the more rostral portions of AI displayed a similar pattern of distribution, with numerous cells clustered along the lateral ventricle in NCLl. Labeled neurons after injection into caudal AI were notably less numerous and rather scattered.

3.4 | HA tracer injections

For retrograde tracing of HA projections, two birds received bilateral CtB injections into HA at either A13.50 or A11.50. With respect to Shimizu et al. (1995), the injection at A13.50 corresponds to the ventral HA, whereas the injection at A11.50 rather corresponds to the dorsal HA. We searched for labeled neurons within the arcopallium, TnA, PoA, and the NCL. Injection sites and the distribution of labeled neurons are illustrated in Figure 9. In case 972 (blue illustrations in Figure 9a and Figure 9b), CtB was injected into HA at A13.50, and in case 062 (red illustrations in Figure 9a and Figure 9c), CtB was injected into HA at A11.50 . In both cases, we observed a similar pattern of retrogradely labeled neurons within NCL between A5.50 and A7.50 (Figure 9d,e) and within the ventral arcopallium (Av) at A6.50. We furthermore detected labeled neurons in the PoA at A6.50 (Figure 9f). We did not observe any labeling in TnA.

3.5 | NCL tracer injections

For anterograde and retrograde tracing of NCL projections, three birds received bilateral CtB injections into the NCL at A6.50. Injections were administered along the mediolateral axis at either L4.00, L6.50, or L8.00. We searched for labeled fibers and neurons within the arcopallium, TnA, PoA, MSt, LSt, anterior nidopallium, and HA. Injection sites and the distribution of labeled neurons and fibers are schematically illustrated in Figures 10a, 11a,b, and 12a,b.

In case 914 (green illustrations in Figures 10–13), CtB was injected at L4.00. A network of anterogradely labeled terminating fibers and retrogradely labeled neurons was observed in AI, AIvm, AIdm, AM, and PoA, ranging from A5.50 to A6.50 (Figure 10b,e). Within the striatum, terminating fibers were predominantly detected in the lateral somatic portion of MSt (sMSt) between A8.50 and A11.50 (Figure 11c,f), which means that the medial limbic portion of MSt was mainly spared. As expected, no labeled neurons were detected within the striatum after NCL injections. Apart from that, extensive retrograde labeling could also be detected in the medial part of the anterior nidopallium (NIM) ranging from A8.50 to A11.50. In the posterior sections between A8.50 and A9.50, the full extent of NIM was covered with labeled cells. For the more anterior sections between A10.50 and A11.50, retrograde labeling was mainly observed in the dorsal part of NIM (Figure 11b,i). Additionally, within HA, neurons as well as fibers were detected throughout the entire rostral extent between A11.50 and A13.50 (Figure 12c,f). Moreover, we found retrogradely labeled neurons within the auditory field L1 (Figure 13a,b).

In case 921 (red illustrations in Figure 10–13), the CtB injection was placed at L6.50. Labeled neurons and fibers were detected within AI between A5.50 and A7.50 (Figure 10c,f). At A5.50, neurons were distributed in a scattered fashion, whereas terminal fibers were clustered in the center of AI. Moreover, fibers were found within TnA. At A6.50, fibers terminated in the medial AI, stretching into AIvm. Labeled

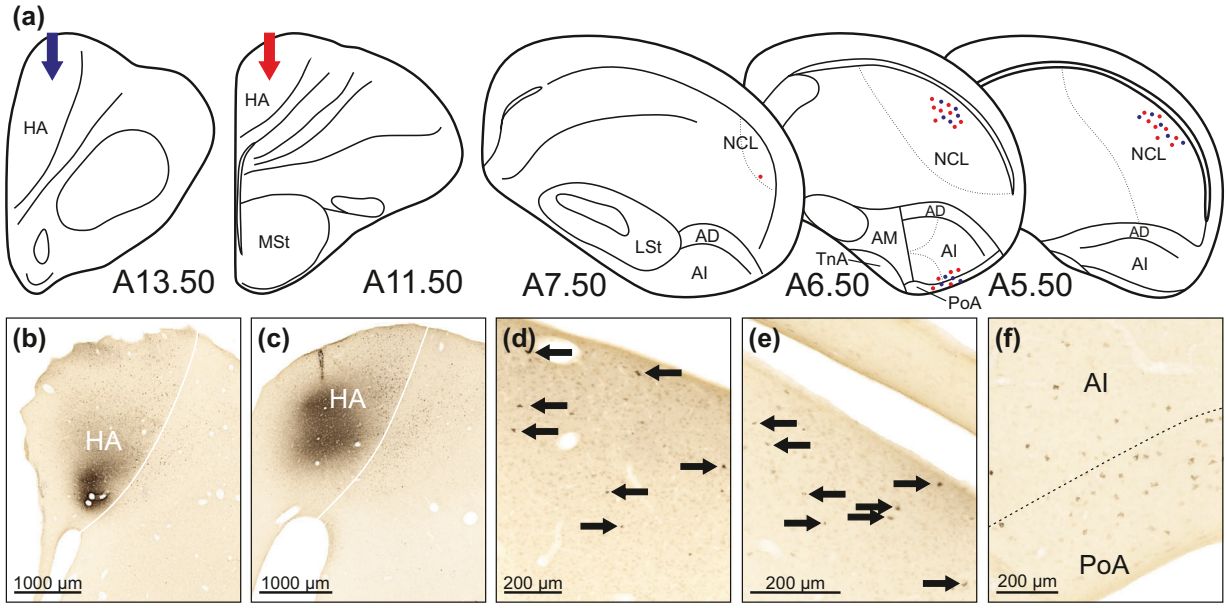

FIGURE 9 Schematic illustration of the hyperpallial injection sites and rostrocaudal extent of retrogradely labeled neurons. (a) The core of the CtB injection site at A13.50 is marked with a blue arrow, whereas the injection site at A11.50 is marked with a red arrow. Blue dots represent retrogradely labeled neurons after injection at A13.50, and red dots represent retrogradely labeled neurons after injection at A11.50. (b) CtB injection site at A13.50 (case 972). (c) CtB injection site at A11.50 (case 062). (d) Labeled neurons in NCLl at A6.50 after CtB injection at A13.50 (case 972). (e) Labeled neurons in NCLl at A6.50 after CtB injection at A11.50 (case 062). (f) Labeled neurons in the ventral AI and PoA at A6.50 after CtB injection at A11.50 (case 062). For abbreviations, see list.

neurons were mainly detected within the ventral portion of AI, but some neurons were also found within AM. Furthermore, there were some terminating fibers found in PoA. At A7.50, terminating fibers were clustered in central AI, while neurons were adjacently clustered in more medial AI. Within the striatum, we detected terminating fibers that ranged from A8.50 to A11.50 and were predominantly located within the somatic portions of MSt and LSt (sLSt). Different densities of labeled fibers revealed a clear border between somatic and limbic portions of the MSt (Figure 11d,g). Moreover, extensive retrograde labeling was found in the anterior nidopallium between A8.50 and A11.50. In the more posterior sections between A8.50 and A9.50, retrograde labeling was rather located within the nidopallium intermedium (NI) dorsal to the entopallium (Figure 13c,d). In the more anterior sections between A10.50 and A11.50, retrograde labeling was most extensive in NIML (Figure 11b,j). Furthermore, the injection also resulted in labeled fibers and neurons within HA, ranging from A11.50 to A13.50 (Figure 12d,g).

In case 959 (blue illustrations in Figure 10–13), CtB was injected into the NCL at L8.00, but tracer spread also included the adjacent nidopallium caudocentrale. A dense network of labeled fibers was found in the lateral portion of AI, ranging from A5.50 to A7.50 (Figure 10d,g). Moreover, few fibers were found within TnA. Labeled neurons were mainly found within the medial portion of AI, spreading into AM. More caudally, at A5.50, neurons were also detected within lateral AI. Within the striatum, most fibers were found within sMSt and sLSt (Figure 11e,h). In comparison to case 921, the density of fibers was slightly increased. After NCL injections, no labeled neurons were detected within the striatum. Moreover, extensive retrograde labeling was found in the anterior nidopallium between A8.50 and A11.50. In the more posterior section between A8.50 and A9.50, retrograde labeling was mainly found in the lateral nidopallium intermedium (NIL), whereas in the anterior sections between A10.50 and A11.50, retrograde labeling was especially strong in NIML (Figure 11b,k). We also found retrogradely labeled neurons within the nidopallium frontotrigeminale (NFT) between A12.00 and A13.00 (Figure 13e,f). Furthermore, within HA, only sparse neurons and thin fibers were found despite a massive injection volume (Figure 12e,h).

Taken together, tracer injections into the NCL revealed a dense network of efferent and afferent connections with several telencephalic structures. Among all examined areas, the connection between the NCL and arcopallium was the most notable with a highly topographic organization of termination fields within the more caudal AI. Ascending projections from the arcopallium to the NCL do not seem to follow this pattern. Concerning areas adjacent to the arcopallium, we found a reciprocal connection to PoA and a few labeled fibers within TnA. The projection pattern to the striatum was also topographic but to a much lesser degree compared to the efferents to the arcopallium. Moreover, we found retrogradely labeled cells within the anterior nidopallium that followed a topographic pattern. The lateral NCL injections resulted in retrograde labeling within NIL and NIML, whereas the more medial NCL injections resulted in retrograde labeling predominantly within NIM and NIML. The intermediate NCL injections on the other hand led to retrograde labeling in NI dorsal to the entopallium and within NIML. We also detected a reciprocal connection between the NCL and HA.

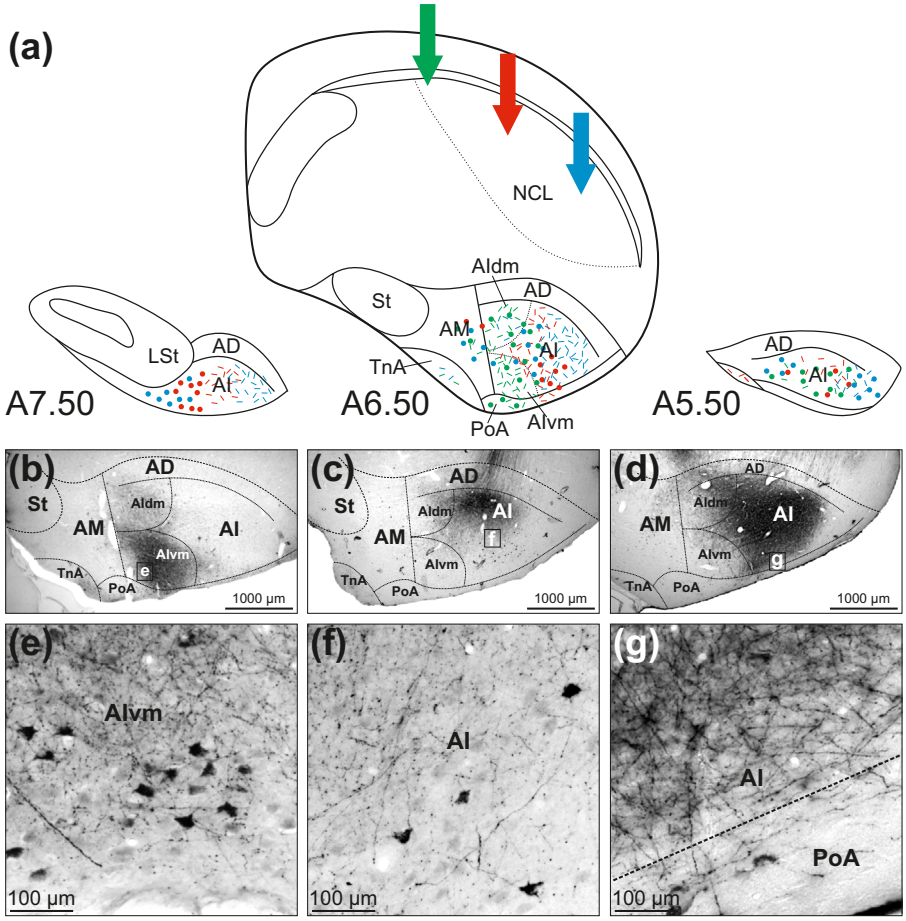

FIGURE 10 Schematic illustration of NCL injection sites and the rostrocaudal extent of retrogradely labeled neurons and anterogradely labeled fibers within the arcopallium and adjacent limbic areas. (a) The core of the NCL injection site is marked by an arrow. Dots represent retrogradely labeled neurons, whereas streaks represent anterogradely labeled fibers. Each animal is allocated a different color for better illustration. Case 914 is illustrated in green (CtB injection at L4.00), case 921 is illustrated in red (CtB injection at L6.50), and case 959 is illustrated in blue (CtB injection at L8.00). (b–d) Labeled neurons and fibers within the arcopallium and the adjacent limbic areas PoA and TnA at A6.50 following NCL injections at L4.00 (b), L6.50 (c), and L8.00 (d). (e) Enlargement of the box depicted in panel (b). Labeled neurons embedded in a fiber network within AIvm at A6.50. (f) Enlargement of the box depicted in panel (c). A fiber network and few labeled neurons in the center of AI at A6.50. (g) Enlargement of the box depicted in panel (d). A dense fiber network in AI at the border to PoA at A6.50. For abbreviations, see list.

3.6 | Morphology and calcium-binding protein expression of NCL projection neurons

To measure soma sizes of the two types of NCL projection neurons (NCL neurons projecting to AI [NCL_{arco}] and NCL neurons projecting to MSt [NCL_{MSt}]), two birds received CtB injections into both the AI of one hemisphere and the MSt of the other. These birds stem from the tracing experiments described above. We found that NCL_{MSt} neurons (9.19 μm^2 ± 2.108 *SD*, N = 2.758) had larger soma diameter than NCL_{arco} neurons (8.64 μm^2 ± 2.078 *SD*, N = 11.666). A multiple linear regression was used to test if "brain area" predicted "soma diameter". We found that the overall regression was statistically significant (F = 46.979, $p < .001$, R^2 = .009). Moreover, we found that "brain area" (β = .064, t = 2.171, p = .030) significantly predicted "soma diameter" after correcting for subject (β = .033, t = 1.247, p = .212) and interaction effects (β = .023, t = 0.561, p = .575) (Figure 14a).

We found that NCL_{MSt} neurons (69.76 μm^2 ± 31.254 *SD*, N = 2.758) had larger somata than NCL_{arco} neurons (61.95 μm^2 ± 30.421 *SD*, N = 11.666). A multiple linear regression was used to test if "brain area" significantly predicted soma area. We found that the overall regression was statistically significant (F = 57.580, $p < .001$, R^2 = .012). Moreover, we found that brain area (β = .069, t = 2.305, p = .021) significantly predicted soma area after correcting for subject (β = .018, t = 0.674, p = .501) and interaction effects (β = .039, t = 0.947, p = .344) (Figure 14b).

Next, we decided to examine whether NCL_{arco} neurons were colocalized with the calcium-binding proteins CB (Figure 15a–c), PV (Figure 15d–f), and CR (Figure 15g–i). In zebra finches, it has been shown that HVC interneurons but not HVC projection neurons express calcium-binding proteins (Wild et al., 2005). We now wanted to investigate whether this also applies to pigeon NCL_{arco} neurons. For this experiment, three birds received unilateral BDA injections into AI. First, we conducted DAB stainings with one brain series of each bird

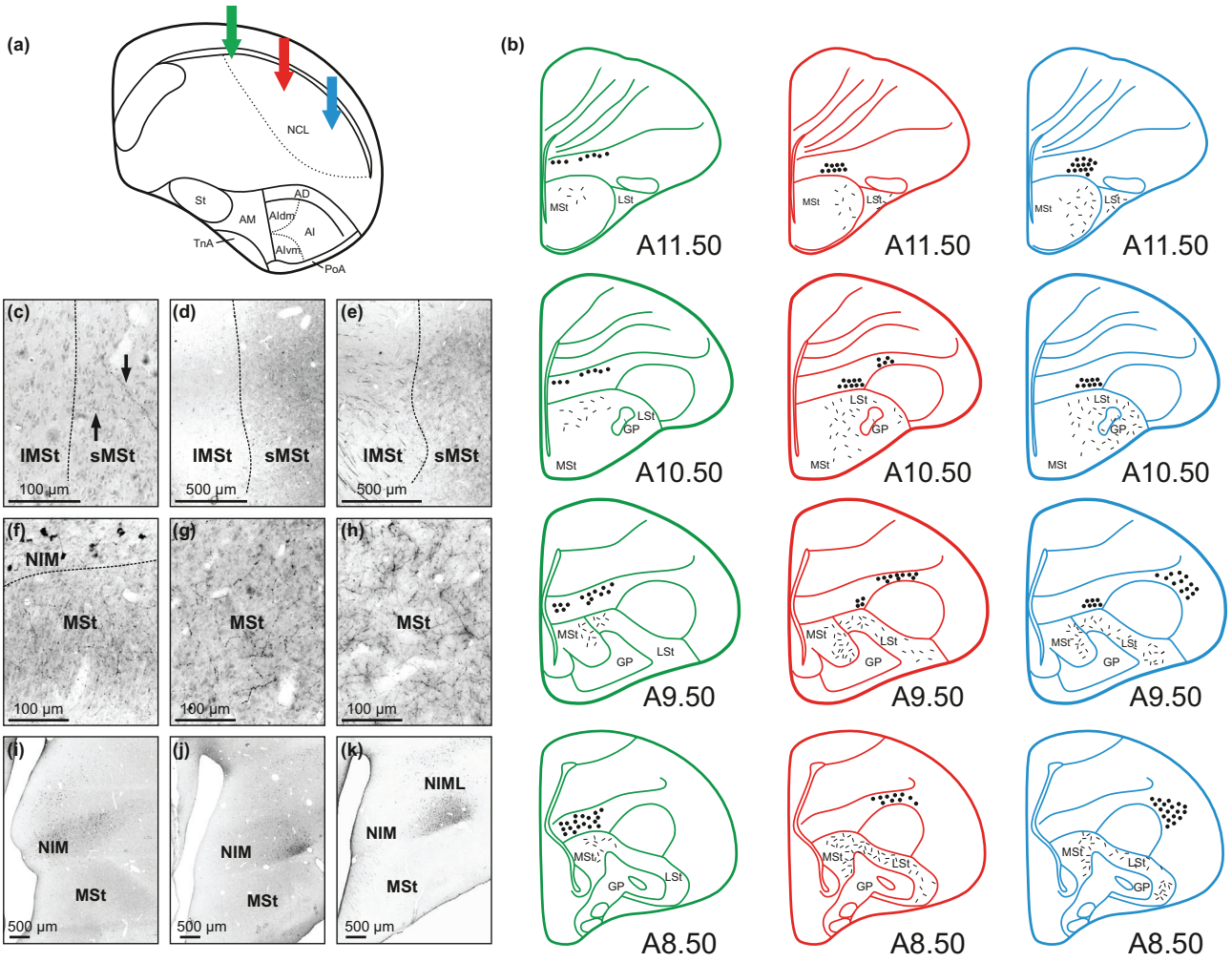

FIGURE 11 Schematic illustration of NCL injection sites and the rostrocaudal extent of anterogradely labeled fibers within the medial and lateral striatum and retrogradely labeled neurons within the nidopallium. (a) The core of the NCL injection site is marked by an arrow. Each animal is allocated a different color for better illustration. Case 914 is illustrated in green (CtB injection at L4.00), case 921 is illustrated in red (CtB injection at L6.50), and case 959 is illustrated in blue (CtB injection at L8.00). (b) Rostrocaudal extent of anterogradely labeled fibers within the medial and lateral striatum and retrogradely labeled neurons within the nidopallium following NCL injections at L4.00 (left green panel), L6.50 (middle red panel), and L8.00 (right blue panel). (c–e) Labeled fibers within the medial striatum at A8.50 following injections at L4.00 (c), L6.50 (d), and L8.00 (e). Dotted lines indicate the border between lMSt and sMSt. (f–h) Labeled fibers within the medial striatum following injections at L4.00 (f), L6.50 (g), and L8.00 (h). (i–k) Retrogradely labeled neurons within NIM and NIML following NCL injections at L4.00 (i), L6.50 (j), and L8.00 (k). For abbreviations, see list.

to check for successful retrograde labelling within NCL. Then, we conducted fluorescence stainings and visualized retrogradely BDA-labeled neurons together with either CB, PV, or CR. We did not observe co-localization of BDA with any of the calcium-binding proteins (Figure 15). As we did not observe CR expression within our retrogradely labeled cluster in the NCL (Figure 15h), we verified our staining in other areas such as LSt, where we detected reliable CR expression (Figure 15j–l).

4 | DISCUSSION

The aim of the present study was to gain detailed insight into the organization of the two descending premotor projections that originate from the multimodal NCL in pigeons. First, we tested whether NCL neurons projecting to MSt and AI are constituted by a single neuronal population with bifurcating neurons, or whether they form two distinct populations as found in songbirds. For that purpose, we injected tracers into MSt and AI and scanned the NCL for double-labeled neurons. We did not find a single bifurcating cell, but instead a remarkably differentiated projection pattern to both target areas. Second, we found morphological differences between the two neuronal populations as NCL_{MSt} neurons possessed significantly larger somata than NCL_{arco} neurons. Moreover, we quantified calcium-binding protein expression of NCL_{arco} neurons and found that they were negative for CB, PV, and CR. Third, we aimed at describing the two descending NCL projections in more detail by examining their topographic organization. For that, we injected tracers into MSt and AI at different stereotactic anteropos-

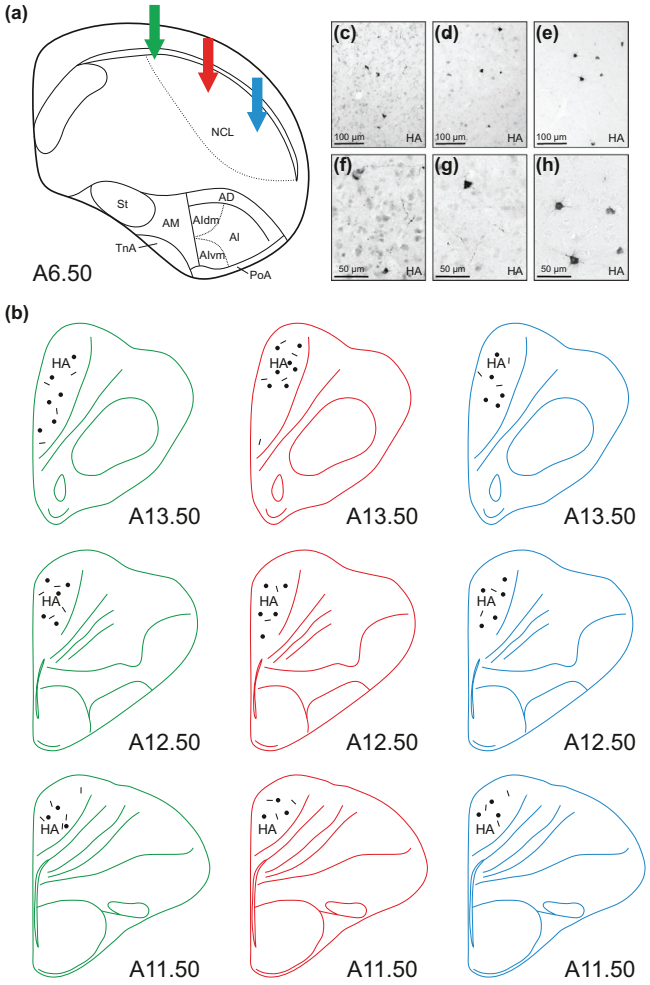

FIGURE 12 Schematic illustration of NCL injection sites and the rostrocaudal extent of retrogradely labeled neurons and anterogradely labeled fibers within HA. (a) The core of the NCL injection site is marked by an arrow. Each animal is allocated a different color for better illustration. Case 914 is illustrated in green (CtB injection at L4.00), case 921 is illustrated in red (CtB injection at L6.50), and case 959 is illustrated in blue (CtB injection at L8.00). (b) Rostrocaudal extent of retrogradely labeled neurons and anterogradely labeled fibers within HA following NCL injections at L4.00 (left green panel), L6.50 (middle red panel), and L8.00 (right blue panel). (c, d) Labeled neurons and fibers within the rostral HA at A12.50 following NCL injections at L4.00 (c), L6.50 (d), and L8.00 (e). (f–h) Enlargement of labeled neurons and fibers following NCL injections at L4.00 (f), L6.50 (g), and L8.00 (h). For abbreviations, see list.

teriorcoordinates and into NCL at different stereotactic mediolateral coordinates. We revealed a weak topographic NCL projection toward the striatum and confirmed a strong topographic organization of the NCL projection toward AI with clearly distinguishable termination fields. Forth, we found reciprocal connections between HA and the entire mediolateral extent of the NCL, and between HA and AI. However, none of these projections were organized in a topographic manner.

4.1 | Distribution and morphology of NCL_{arco} and NCL_{MSt} projection neurons

The major aim of this study was to examine the descending premotor projections of the NCL and to find out whether the projections to the arcopallium and striatum are anatomically separated within the NCL. By doing so, we explored a possible evolutionary scenario in which the pigeon premotor projections possibly resemble the ancient avian neural precursor for the derived and specialized oscine song system. We administered injections into the arcopallium and striatum and analyzed retrograde labeling within the NCL. Even though the NCL does not encompass any clearly visible cytoarchitectonic subdivisions, Herold et al. (2011) proposed a medial/lateral division based on receptor fingerprint patterns. Accordingly, the lateral NCL (NCLl) refers to the NCL portion close to the ventricle where input from all secondary sensory areas arrives and arcopallial projections emanate, whereas the medial NCL (NCLm) lies more inward and mainly harbors neurons with striatal projections (Kröner & Güntürkün, 1999). We verified that MSt projection neurons predominantly occupied NCLm, resembling frontostriatal circuits, while arcopallial projection neurons were mostly located in NCLl, with only a small area of overlap between these divisions. These findings are in line with earlier tracing studies that also suggested that the NCL is divisible into a medial and a lateral projection field (Kröner & Güntürkün, 1999). Using double tracing techniques, we now could show that NCLm and NCLl neurons with striatal and arcopallial projections, respectively, constitute two separate populations.

Since these two populations resemble the pattern of AFP and PMP neurons in songbirds, we wanted to know if the morphological differences known for HVC_{RA} and HVC_X neurons also exist for NCL_{arco} and NCL_{MSt} neurons. Indeed, we found that on average, NCL_{MSt} neurons possess larger somata than NCL_{arco} neurons. This finding is in line with songbird studies as multiple authors found HVC_X cells to be larger than HVC_{RA} neurons (Katz & Gurney, 1981; Mooney, 2000; Nixdorf et al., 1989; Paton et al., 1985; Wild et al., 2005). Although the absolute cell sizes differ between species (e.g., canaries overall have smaller cells than zebra finches), the relative differences between HVC_{RA} and HVC_X neurons remain constant (Mooney, 2000; Paton et al., 1985; Wild et al., 2005). This also holds true for pigeon NCL projection neurons that are mostly smaller than those in the zebra finch HVC and more comparable to canary HVC projection neurons. Furthermore, we found that cell size distributions of both types of NCL projection neurons overlapped considerably as is the case for zebra finch HVC neurons (Paton et al., 1985; Wild et al., 2005). Soma size positively correlates with axon length (Cullheim, 1978; Lee et al., 1986). If this holds true for NCL neurons, we presume that the larger NCL_{MSt} neurons have longer axons as the distance between NCL and MSt is substantially longer than between NCL and AI. Furthermore, differently sized neurons often vary in multiple other morphological characteristics such as diameter, membrane surface, or combined length of their dendrites, number of terminations, and the shape of the three-dimensional space that their dendritic trees occupy (Cullheim et al., 1987a, 1987b). These morphological differences between neurons are also critically linked to their function

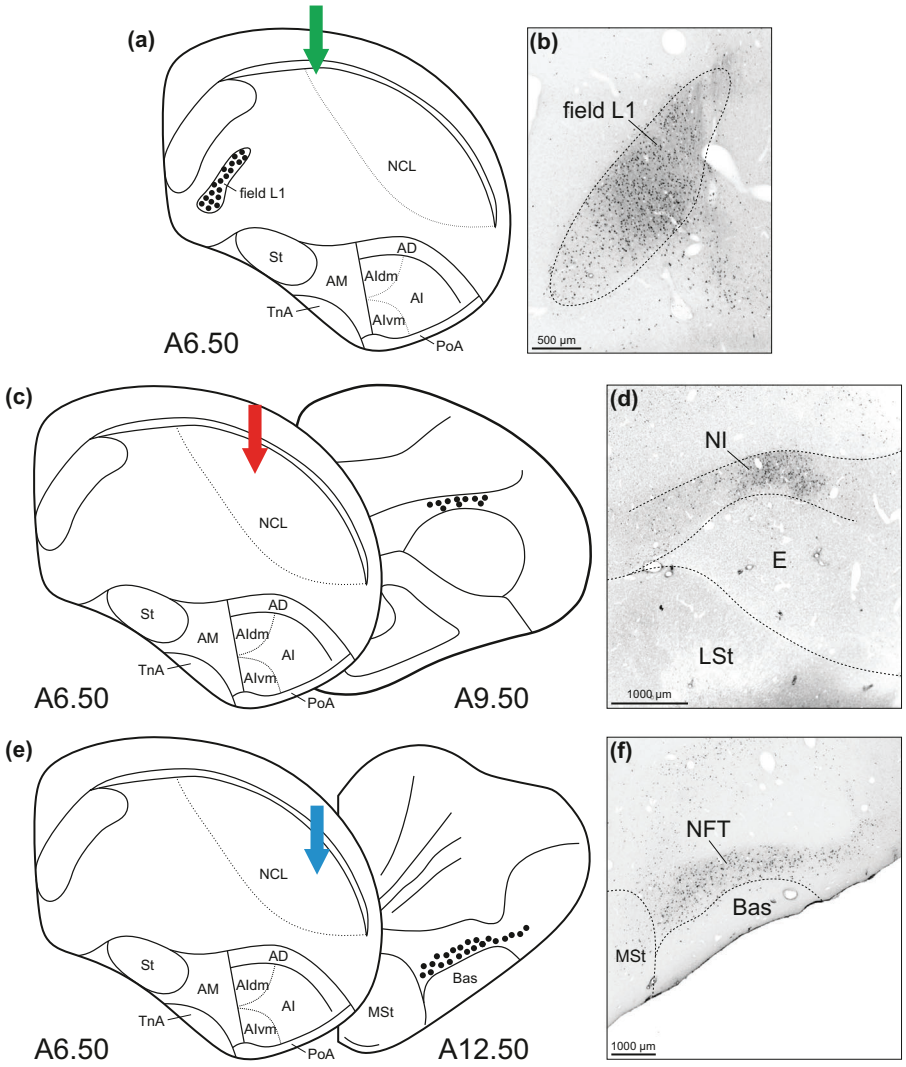

FIGURE 13 Nidopallial injection sites and retrogradely labeled neurons within the auditory field L1, visual NI, and trigeminal NFT. (a) Schematic illustration of the CtB injection site into the dorsomedial tip of the NCL at L4.00 and retrogradely labeled neurons within field L1. (b) Retrogradely labeled neurons within field L1. (c) Schematic illustration of the CtB injection site into the NCL at L6.50 and retrogradely labeled neurons within visual NI. (d) Retrogradely labeled neurons within NI. (e) Schematic illustration of the CtB injection site into the NCL at L8.00 and retrogradely labeled neurons within the trigeminal NFT. (f) Retrogradely labeled neurons within NFT. For abbreviations, see list.

(Brown et al., 2008). Hence, the size difference of the NCL projection neurons is a hint for distinct functions of the two pathways as was already shown in songbirds by in vivo and in vitro electrophysiological studies (Daou et al., 2013; Peng et al., 2012).

In addition to labeled neurons within NCLm, we found extensive retrograde labeling within the anterior nidopallium following MSt injections. These cell clusters were mainly found in NIML, which is consistent with findings of earlier studies (Kröner & Güntürkün, 1999), overall confirming a projection similar to the LMAN–Area X connection of the AFP in songbirds (Figure 1a). Moreover, we revealed a reciprocal connection between the rostral part of HA and the NCL (Figure 12a,b) as well as descending projections from rostral HA to rostral AI (Figure 7) and to MSt (Figure 4). The most rostral part of HA is assumed to be comparable to the primary motor cortex (M1) in mammals (Medina & Reiner, 2000) and receives input from the thalamic ventrointermediate area (VIA), which in turn receives input from the SNr, deep cerebellar nuclei, and the dorsal pallidum (Medina & Reiner, 1997; Medina et al., 1997). This pallido–VIA–HA pathway seems to resemble the pallido-thalamo-motor-cortical loop of mammals (Medina & Reiner, 1997, 2000). As the rostral HA targets premotor brainstem areas including the nucleus ruber (Wild, 1992), our findings indeed contribute to the idea that the rostral HA resembles the mammalian motor cortex (Wild & Williams, 2000).

4.2 | Modality-specific pallio-motor loops

A further aim of the current study was to analyze the topography of the scrutinized projections. We were able to discern distinct projection fields with NCL_{MSt} neurons clustering predominantly in NCLm

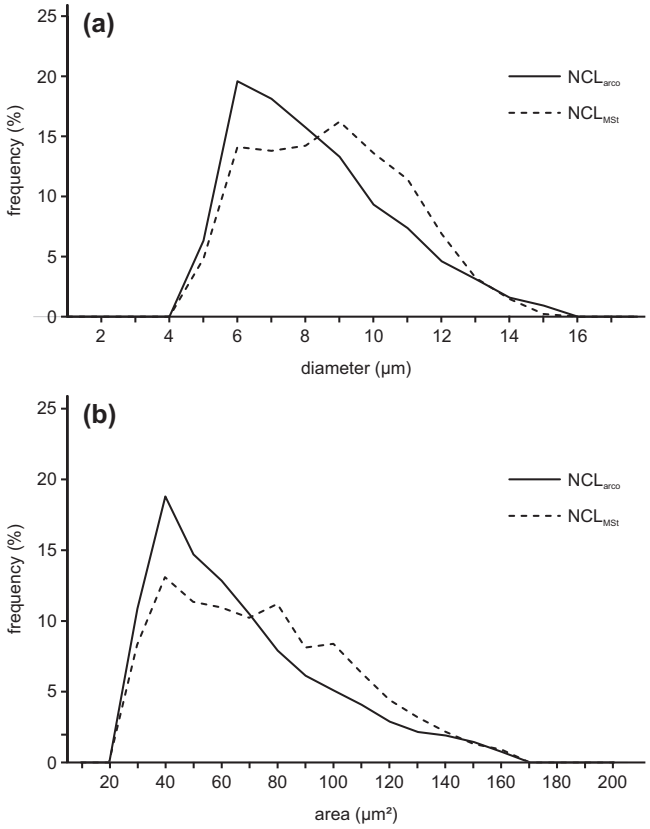

FIGURE 14 Relative frequency distributions of the sizes of CtB-labeled NCL projection neurons. (a) Frequency distributions of the diameter of retrogradely labeled NCL neurons projecting to either AI (NCL_{arco}) or MSt (NCL_{MSt}). (b) Frequency distributions of the area of retrogradely labeled NCL neurons projecting to either AI (NCL_{arco}) or MSt (NCL_{MSt}). The ordinate depicts the relative frequency of measured cells at the sizes depicted on the abscissa.

and NCL_{arco} neurons in NCLl along the ventricle. Next, we investigated the input from the NCL to the arcopallium more thoroughly and found that the termination fields within AI were clearly distinguishable (Figure 10a), thereby confirming recent findings by Fernández, Morales, et al. (2020) and other tracing studies. These studies found that the dorsomedial NCL sends auditory information to the medial part of AI (Fernández, Morales, et al., 2020; Wild et al., 1993), whereas the central part of NCL relays visual information to the central AI (Fernández, Morales, et al., 2020). Finally, the lateral NCL provides trigeminal input to the lateral part of AI (Wild & Farabaugh, 1996; Wild et al., 1985). A similar organization of NCL efferents has also been demonstrated in songbirds (Paterson & Bottjer, 2017). The authors showed that arcopallial termination fields of projections from the dorsal NCL (dNCL) are located within the dorsal AI (AId), evading the song nucleus RA, and then converge onto the Av. The projection from HVC to RA, while not being organized topographically in itself (Foster & Bottjer, 1998), adds a further stream more medial to the above-described topography that is exclusive to vocal learning species. Thus, projections from HVC and the adjacent visual and trigeminal NCL terminate in a similar mediolateral topography across RA and AId (Bottjer et al., 2000; Mello et al., 1998; Wild & Farabaugh, 1996). Overall, the organization of arcopallial afferents in songbirds seems to mimic the parallel arrangement found in pigeons.

Our work also contributes to studies of the arcopallium that demonstrated that AI and AD receive projections from higher associative pallial areas as well as from primary sensory areas (Dubbeldam & Visser, 1987; Fernández, Morales, et al., 2020; Kröner & Güntürkün, 1999; Shanahan et al., 2013; Wild et al., 1985, 1993; Zeier & Karten, 1971). These studies found that the nidopallial areas surrounding the primary sensory pallial areas of the auditory, visual, and trigeminal pathways project to specific arcopallial regions both directly and indirectly via relay stations in the NCL (Bottjer et al., 2000; Cohen et al., 1998; Dubbeldam & Visser, 1987; Fernández, Morales, et al., 2020; Kröner & Güntürkün, 1999; Leutgeb et al., 1996; Metzger et al., 1998; Wild & Farabaugh, 1996). Our study confirmed these nidopallial origins of secondary sensory input into the NCL as we revealed projections from the auditory field L1 to the dorsomedial NCL (Figure 13a,b), from the visual NI to the central NCL (Figure 13c,d), and from the trigeminal NFT to the lateral NCL (Figure 13e,f). It is known that field L receives input from the dorsal nucleus mesencephalicus lateralis (MLd) via the nucleus ovoidalis (Ov) (Karten, 1967; Wild et al., 1993; Figure 16, green panel), and NI receives visual input from the entopallium, which in turn receives afferents from the optic tectum (TeO) via the nucleus rotundus (Rt) (Fernández, Ahumada-Galleguillos, et al., 2020; Husband & Shimizu, 1999; Karten & Hodos, 1970; Krützfeldt & Wild, 2005; Figure 16, red panel). NFT receives direct trigeminal input from the principal sensory trigeminal brainstem nucleus (PrV) (Kobylkov et al., 2020) but also indirect input via the nucleus basalis (Fernández et al., 2021; Wild et al., 1985; Figure 16, blue panel). Interestingly, the separate AI zones send descending projections through the OM and target the specific nuclei within the brainstem, midbrain, and thalamus that give rise to the described ascending sensory pathways. In particular, the auditory AI targets the surrounding areas of Ov and MLd, the visual AI targets the surrounding areas of Rt and TeO, and the trigeminal AI targets the surrounding area of PrV (Fernández, Morales, et al., 2020; Wild et al., 1993). These surrounding areas then project back to their respective core nucleus, thereby forming closed and topographically organized modality-specific loops (Figure 16).

A further finding of our tracing experiments was a weak topographic organization of the NCL projections toward the striatum (Figure 11). The avian striatum encompasses a medial (MSt) and lateral part (LSt) and receives input from several pallial somatic as well as limbic structures (Kuenzel et al., 2011; Wild, 1987). It is known from other tracing studies that limbic afferents reach the most medial portion of the MSt, whereas somatic afferents reach the lateral two third of MSt and most of LSt (Kuenzel et al., 2011; Veenman et al., 1995). Our findings resemble this border between limbic and somatic striatum as the termination field of auditory NCL efferents was restricted to lMSt, whereas visual and trigeminal termination fields rather occupied sMSt and LSt (Figure 11). However, the overall topography of NCL_{MSt} projections was by far not as pronounced as found for NCL_{arco} projections. We were especially not able to distinguish between visual and trigeminal termination fields. This is in line with the idea of Alexander et al. (1986)

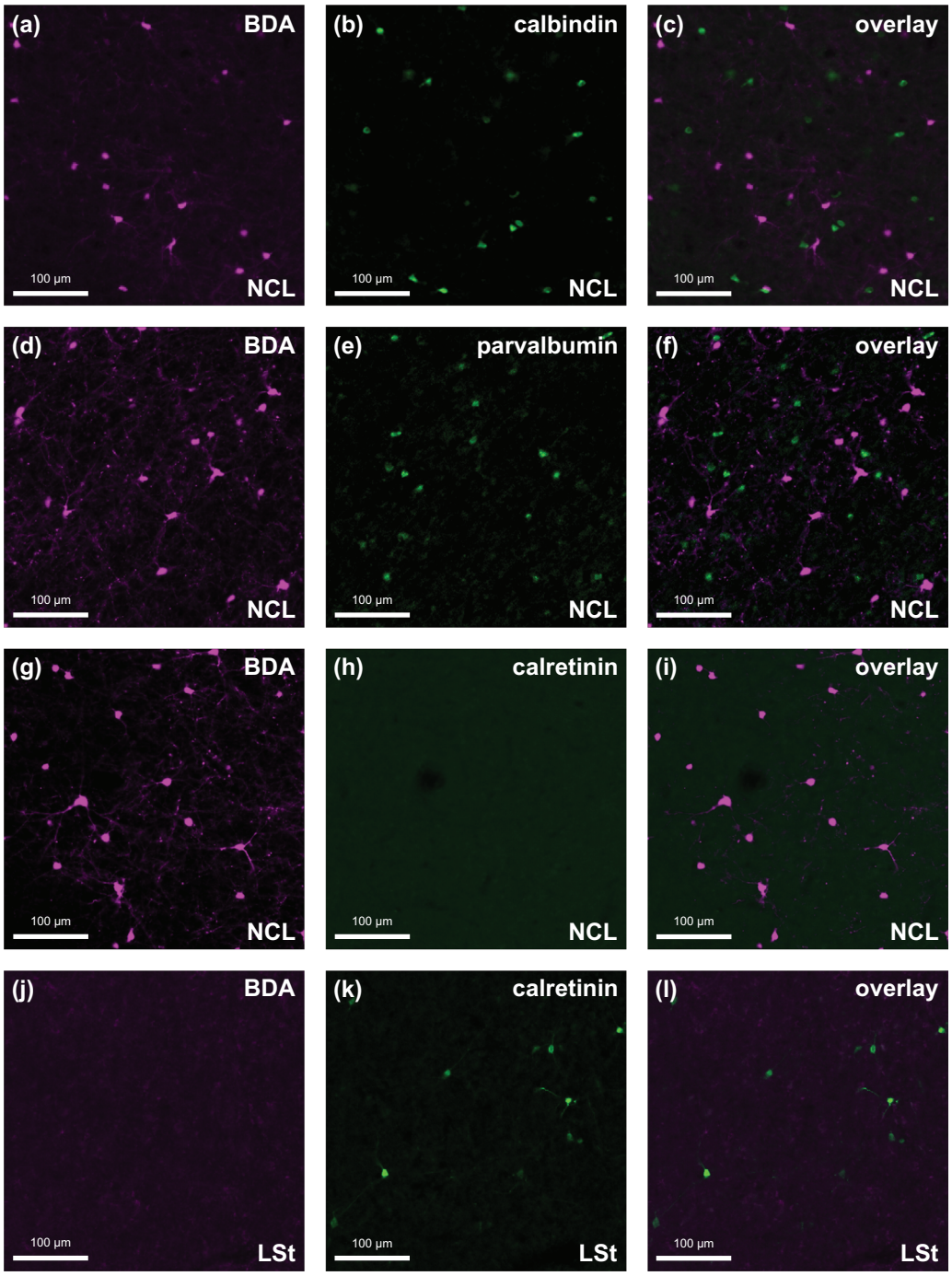

FIGURE 15 Overlay of retrogradely BDA-labeled NCL_{arco} neurons with CB, PV, and CR. (a, d, g) Retrogradely labeled neurons within NCL after BDA injection into AI. (b, e, h) Neurons positive for either CB, PV, or CR, respectively, at the same site. Note that no CR-positive neurons were found within our retrogradely labeled cluster in the NCL. (c, f, i) No overlay of NCL_{arco} neurons with any of the calcium-binding proteins was detected. (j–l) To show that the CR staining itself was successful, however, we included pictures from the LSt within the same slice, where we found CR-positive neurons. Overall, no NCL_{arco} neuron was positive for any of the tested calcium-binding proteins. For abbreviations, see list.

who proposed a generalized model of mammalian cortico-striato-pallidal-thalamo-cortical loops with an aggregating convergence of cortical inputs along the circuit. While distinct pallial areas project to partially overlapping portions of the striatum, these striatal areas send further converging efferents to the GP and SNr, which in turn project to restricted nuclei within the thalamus. Similarly, the avian striatum receives afferents from many different regions of the pallium including the higher associative areas NCL and NIML (Kröner & Güntürkün, 1999; Veenman et al., 1995). The information from the striatum is then further relayed via the GP and SNr to the thalamus (Jiao et al.,

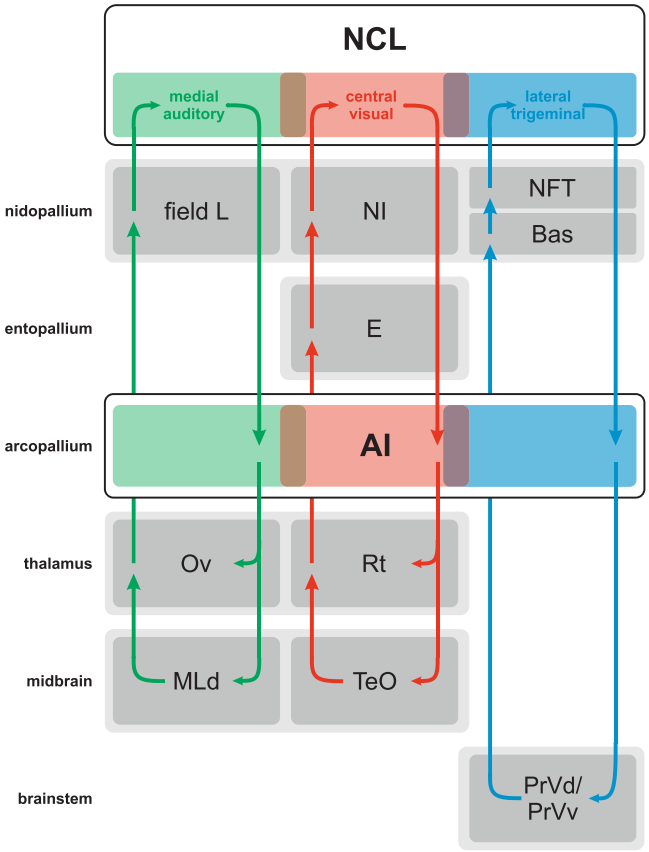

FIGURE 16 Simplified illustration of parallel modality-specific pallio-motor loops in the pigeon brain. Ascending auditory (green), visual (red), and trigeminal (blue) inputs reach the NCL in a medial-to-lateral topography via modality-specific relay stations in the brainstem, midbrain, thalamus, and pallium. Moreover, the NCL sends modality-specific output to AI in the same medial-to-lateral organization. The AI in turn sends efferents via the OM back to the specific sensory structures that form the origins of the ascending pathways, thus closing the modality-specific parallel loops. To be exact, OM fibers do not terminate directly in Ov, MLd, Rt, and TeO, but in adjacent areas surrounding the respective nuclei (Fernández, Morales, et al., 2020; Wild et al., 1993). For better illustration, this is not depicted here. Note that Kobylkov et al. (2020) recently identified a new direct connection between PrVv and NFT, which is not depicted here. For abbreviations, see list.

2000). Finally, the thalamus projects back to the NCL and NIML (Kitt & Brauth, 1982; Kröner & Güntürkün, 1999). Overall, this circuit resembles cortico-striato-thalamo-cortical loops in mammals. Nevertheless, these loops are not modality specific and therefore not comparable to the above-described parallel pallio-motor loops involving arcopallial projections.

Our findings also revealed that HA is linked to each of the three modality-specific pallio-motor loops via its reciprocal connections with the auditory, visual, and trigeminal NCL. Moreover, we found a reciprocal connection with AI and a descending projection to the striatum, thereby confirming earlier tracing studies (Kröner & Güntürkün, 1999; Veenman et al., 1995). Overall, our data indicate that HA can interact with the pallio-motor loops at various stages. Beyond our findings, earlier experiments demonstrated that especially the tectofugal visual stream is directly influenced by HA via the tractus septo-mesencephalicus (TSM), which innervates the deep layers of TeO (Adamo, 1967; Karten et al., 1973; Kröner & Güntürkün, 1999; Miceli et al., 1987). These HA efferents modulate tectal and rotundal activity as shown by visual wulst stimulation as well as inactivation (Bagnoli et al., 1977, 1979; Britto, 1978; Folta et al., 2004, 2007). The deep layers of TeO give rise to descending tectomotor output projections but also innervate Rt (Hellmann et al., 2004), which in turn sends ascending information to the entopallium (Figure 16). Thus, both the ascending pathway to the Rt (Folta et al., 2004) and the descending tectomotor output pathways (Folta et al., 2007) are influenced via the TSM.

Moreover, we revealed that input from the anterior forebrain to NCL is organized in a topographic manner. We found that the medial NCL receives input from the medial NI (NIM) and NIML, the central NCL is strongly innervated by neurons from NI dorsal to the entopallium and NIML, and the lateral NCL receives its input from the more lateral NI (NIL) and NIML. This is in line with other tracing studies that found that the NI–NCL connection is reciprocal and topographic along both the anteroposterior as well as the mediolateral axis (Fernández, Ahumada-Galleguillos, et al., 2020; Kröner & Güntürkün, 1999). Within NI, NIML is regarded as comparable to the song nucleus LMAN. Even though there is no direct connection between LMAN and HVC, a reciprocal and topographically organized connection exists between LMAN and dNCL, which is adjacent to HVC (Paterson & Bottjer, 2017). In this respect, NIML and LMAN share a similar anatomical location and connectivity within the nidopallium, but whether they also share functional properties needs further investigation. The few existing behavioral studies on NIML function suggest that the nucleus is involved in executing sequential behavior (Hahn & Rose, 2023; Helduser & Güntürkün, 2012; Helduser et al., 2013; Rook, Tuff, Packheiser, et al., 2021) but does not modulate the variability of behavior (Helduser et al., 2014) as it is suggested for LMAN (Hampton et al., 2009).

4.3 | Evolutionary considerations and comparison to the oscine brain

A main aim of this study was to examine a possible evolutionary scenario in which a basic avian motor system developed into a more specialized song system. Among all avian vocal learners (songbirds, hummingbirds, and parrots), the two song pathways exhibit striking similarities and as a conclusion, it was hypothesized that these pathways have evolved independently under strong genetic and epigenetic constraints from a preexistent motor pathway (Feenders et al., 2008; Jarvis, 2019). Feenders et al. (2008) corroborated their hypothesis by demonstrating that movement-associated areas in male songbirds are directly adjacent to the vocal nuclei. Thus, it is plausible that within the oscine song system, HVC projections to the Area X within MSt (AFP) and to RA within the arcopallium (PMP) have developed from more diffuse NCL projections toward the striatum and arcopallium as found in nonvocal learners.

Ebbesson (1980) proposed that neuronal specialization is achieved by a process that he called parcellation. He assumed that in the beginning of vertebrate evolution, neural systems were rather diffuse, undifferentiated, and richly interconnected. In conjunction with the development of complex behaviors, these systems became increasingly structured during evolution by the selective loss of previous connections and the aggregation of subsystems. Selective pressures could then have regulated the precise degree of parcellation in a given organism. Studies showed that within oscine HVC, projection neurons target either Area X or RA, but have no other efferent connections (Mooney & Prather, 2005; Nottebohm et al., 1982). If we suppose that these specialized neurons evolved by parcellation, we could conclude that in less differentiated avian brains, biprojecting neurons might occur within an area overlapping with HVC. These neurons might constitute a preliminary stage of the more specialized neurons we observe within the oscine song system. However, we did not find biprojecting neurons within the NCL of nonvocal learning pigeons, but instead a differentiated projection pattern in which two distinct neuronal populations target either the striatum or the arcopallium. We conclude that it is unlikely that the oscine song system has evolved by parcellation in sensu (Ebbesson, 1980).

For an alternative explanation, it is conceivable that HVC neurons have evolved via other yet unknown mechanisms. Possibly, pigeon NCL projection neurons do not constitute a more primitive precursor system but are already specialized to serve particular functions that differ from the oscine song system. In a revised scenario, HVC neurons might have evolved from ancestral motor circuits through duplication (Chakraborty & Jarvis, 2015) or the strengthening of these pathways (Petkov & Jarvis, 2012) that later specialized for vocal control (Feenders et al., 2008). This idea is supported by our finding that HVC and NCL projection neurons share a similar connectivity as well as neurochemical and morphological features.

Regarding its connectivity, the auditory dorsomedial tip of the NCL is particularly interesting as it assumes a similar anatomical position as HVC (Farries, 2004). The nonoscine auditory NCL and oscine HVC, especially its surrounding shelf region, display similar projection patterns as they both have reciprocal connections to the auditory field L-complex and the caudomedial nidopallium (Shaevitz & Theunissen, 2007; Shanahan et al., 2013), and send output to AIvm, which in turn sends projections to thalamic and midbrain auditory centers (Mello et al., 1998; Wild et al., 1993). It has been suggested that the circuit between the oscine HVC shelf and RA shelf, called RA cup, is homologous to the nonoscine projection from the auditory NCL to AIdm/AIvm (Vates et al., 1996). This comparison is also supported by similar descending projections of oscine RA and nonoscine AIdm/AIvm as they both target the nucleus intercollicularis (ICo), the lateral mesencephalic nucleus, and the shell region of the Ov (Vates et al., 1996; Wagner et al., 2003; Wild et al., 1993). However, there are also some downstream projections that are exclusive to RA. For example, while RA neurons target the dorsomedial nucleus of ICo (DM) (Amador et al., 2017; Horita et al., 2012; Jarvis et al., 1998; Wild et al., 1997), RA cup projects to the surrounding area of DM within ICo comparable to the auditory arcopallium in pigeons (Mello et al., 1998). This separation within a core and shell region is not only observed in HVC and RA but also for LMAN and Area X (Bottjer & Altenau, 2010; Bottjer et al., 2000; Feenders et al., 2008; Jarvis et al., 2013; Mello et al., 1998). It seems that especially the connections of the shell regions are comparable between vocal learners and nonlearners, suggesting that the shell circuits might be the ancestral condition from which the core circuits evolved in songbirds (Fernández, Morales, et al., 2020). In this regard, the HVC projection to RA might be a subdivision of the HVC shelf–AId circuit that has specialized for vocal control (Farries, 2001). This idea is also supported by neurochemical similarities between these areas as it was, for example, shown that AId and RA share various molecular markers (Mello et al., 2019; Nevue et al., 2020). Similarly, NCL and AI as well as HVC and RA express Cadherin-6B, suggesting that this expression is conserved between vocal learners and nonlearners (Matsunaga et al., 2008; Redies et al., 2001). Additionally, also the HVC_{RA} projection neurons and NCL_{arco} projection neurons seem to have neurochemical similarities. We could not detect any NCL_{arco} neurons in pigeons that express CB, PV, or CR just as it is known that HVC_{RA} neurons seem to be negative for these calcium-binding proteins in songbirds (Wild et al., 2005). In birds, CB-positive neurons, for example, have been detected in the auditory system (Kenigfest et al., 2017; Pinaud et al., 2006), in the hippocampus (Montagnese et al., 1993; Rook et al., 2023), and in the visual system (Heyers et al., 2008). Here, dominant CB expression was found in structures belonging to the thalamofugal pathway but not in the tectofugal pathway, suggesting a function-selective expression pattern. The conserved expression of Cadherin-6B and the seeming absence of calcium-binding proteins in both HVC_{RA} and NCL_{arco} neurons support the idea that the HVC–RA pathway might have evolved from the NCL–AI pathway.

Nonetheless, we want to note that our evolutionary considerations must be regarded with caution as we only investigated one representative of nonvocal learners (pigeons) and compared our results to literature on mainly one representative of vocal learners (zebra finches). To draw more generalized conclusions that apply to the entire groups of vocal nonlearners and learners, more species of both groups should be investigated. Although different bird species share fundamental principles of NCL organization such as its position within the pallium or the occurrence of dopaminergic baskets, more subtle features such as the size and position of subdivisions were shown to vary between chickens and pigeons (nonvocal learners) as well as between zebra finches and crows (vocal learners; von Eugen et al., 2020). Thus, it is conceivable that the NCL might also differ in other aspects between representatives of the same group.

5 | CONCLUSION

The present study demonstrates that the intratelencephalic premotor connections in pigeons are highly organized. While topographic NCL–AI projections are embedded within a system of parallel modality-specific motor loops, such a modality specificity is not present for NCL–striatum projections. From an evolutionary perspective, we conclude that NCL projection neurons do not seem to constitute a

preliminary state of specialized neurons as found in the oscine HVC, thereby contradicting the parcellation theory. Instead, they appear to be already specialized in a fashion that serves particular functions. Novel techniques such as optogenetics that were recently made available in birds (Roberts et al., 2012; Rook, Tuff, Isparta, et al., 2021) can shed light on the different roles of NCL and HVC projection neurons. Overall, our study indicates that the auditory NCL, NIML, and AId of nonvocal learning pigeons resemble the oscine HVC/dNCL, LMAN, and RA cup regions, respectively, based on their connectivity.

ACKNOWLEDGMENTS

This study was funded by the Deutsche Forschungsgemeinschaft (DFG, German Research Foundation) through SFB1280 Project-ID 316803389 subproject A01 and SFB1372 Project-ID 395940726 subproject Neu04.

DATA AVAILABILITY STATEMENT

The data that support the findings of this study are available from the corresponding author upon reasonable request.

ORCID

Noemi Rook https://orcid.org/0000-0002-2415-2813

PEER REVIEW

The peer review history for this article is available at https://publons.com/publon/10.1002/cne.25611.

REFERENCES

Adamo, N. J. (1967). Connections of efferent fibers from hyperstriatal areas in chicken, raven, and African lovebird. *Journal of Comparative Neurology*, *131*(3), 337–355. https://doi.org/10.1002/cne.901310304

Ahumada-Galleguillos, P., Fernández, M., Marin, G. J., Letelier, J. C., & Mpodozis, J. (2015). Anatomical organization of the visual dorsal ventricular ridge in the chick (*Gallus gallus*): Layers and columns in the avian pallium. *The Journal of Comparative Neurology*, *523*(17), 2618–2636. https://doi.org/10.1002/cne.23808

Alexander, G. E., DeLong, M. R., & Strick, P. L. (1986). Parallel organization of functionally segregated circuits linking basal ganglia and cortex. *Annual Review of Neuroscience*, *9*(1), 357–381. https://doi.org/10.1146/annurev.ne.09.030186.002041

Amador, A., Boari, S., & Mindlin, G. B. (2017). From perception to action in songbird production: Dynamics of a whole loop. *Current Opinion in Systems Biology*, *3*, 30–35. https://doi.org/10.1016/j.coisb.2017.03.004

Anderson, C., Parra, R. S., Chapman, H., Steinemer, A., Porter, B., & Colombo, M. (2020). Pigeon nidopallium caudolaterale, entopallium, and mesopallium ventrolaterale neural responses during categorisation of Monet and Picasso paintings. *Scientific Reports*, *10*(1), 15971. https://doi.org/10.1038/s41598-020-72650-y

Bagnoli, B., Francesconi, W., & Magni, F. (1977). Visual wulst influences on the optic tectum of the pigeon. *Brain Behavior and Evolution*, *14*(3), 217–237. https://doi.org/10.1159/000125662

Bagnoli, P., Francesconi, W., & Magni, F. (1979). Interaction of optic tract and visual wulst impulses on single units of the pigeon's optic tectum. *Brain Behavior and Evolution*, *16*(1), 19–37. https://doi.org/10.1159/000121821

Balakhonov, D., & Rose, J. (2017). Crows rival monkeys in cognitive capacity. *Scientific Reports*, *7*(1), 8809. https://doi.org/10.1038/s41598-017-09400-0

Benezra, S. E., Narayanan, R. T., Egger, R., Oberlaender, M., & Long, M. A. (2018). Morphological characterization of HVC projection neurons in the zebra finch (*Taeniopygia guttata*). *The Journal of Comparative Neurology*, *526*(10), 1673–1689. https://doi.org/10.1002/cne.24437

Bolhuis, J. J., Okanoya, K., & Scharff, C. (2010). Twitter evolution: Converging mechanisms in birdsong and human speech. *Nature Reviews Neuroscience*, *11*(11), 747–759. https://doi.org/10.1038/nrn2931

Bottjer, S. W., & Altenau, B. (2010). Parallel pathways for vocal learning in basal ganglia of songbirds. *Nature Neuroscience*, *13*(2), 153–155. https://doi.org/10.1038/nn.2472

Bottjer, S. W., Brady, J. D., & Cribbs, B. (2000). Connections of a motor cortical region in zebra finches: Relation to pathways for vocal learning. *Journal of Comparative Neurology*, *420*(2), 244–260. https://doi.org/10.1002/(SICI)1096-9861(20000501)420:2⟨244::AID-CNE7⟩3.0.CO;2-M

Brenowitz, E. A., Margoliash, D., & Nordeen, K. W. (1997). An introduction to birdsong and the avian song system. *Journal of Neurobiology*, *33*(5), 495–500.

Britto, L. R. (1978). Inhibition of tectal neurons from telencephalic visual areas in pigeons. *Revista Brasileira De Pesquisas Medicas E Biologicas*, *11*(4-5), 223–227.

Brown, K. M., Gillette, T. A., & Ascoli, G. A. (2008). Quantifying neuronal size: Summing up trees and splitting the branch difference. *Seminars in Cell & Developmental Biology*, *19*(6), 485–493. https://doi.org/10.1016/j.semcdb.2008.08.005

Butler, A. B., Reiner, A., & Karten, H. J. (2011). Evolution of the amniote pallium and the origins of mammalian neocortex. *Annals of the New York Academy of Sciences*, *1225*, 14–27. https://doi.org/10.1111/j.1749-6632.2011.06006.x

Chakraborty, M., & Jarvis, E. D. (2015). Brain evolution by brain pathway duplication. Philosophical Transactions of the Royal Society of London. *Series B, Biological Sciences*, *370*(1684), 20150056. https://doi.org/10.1098/rstb.2015.0056

Clayton, N. S., & Emery, N. J. (2015). Avian models for human cognitive neuroscience: A proposal. *Neuron*, *86*(6), 1330–1342. https://doi.org/10.1016/j.neuron.2015.04.024

Cohen, Y. E., Miller, G. L., & Knudsen, E. I. (1998). Forebrain pathway for auditory space processing in the barn owl. *Journal of Neurophysiology*, *79*(2), 891–902. https://doi.org/10.1152/jn.1998.79.2.891

Cullheim, S. (1978). Relations between cell body size, axon diameter and axon conduction velocity of cat sciatic alpha-motoneurons stained with horseradish peroxidase. *Neuroscience Letters*, *8*(1), 17–20. https://doi.org/10.1016/0304-3940(78)90090-3

Cullheim, S., Fleshman, J. W., Glenn, L. L., & Burke, R. E. (1987a). Membrane area and dendritic structure in type-identified triceps surae alpha motoneurons. *Journal of Comparative Neurology*, *255*(1), 68–81. https://doi.org/10.1002/cne.902550106

Cullheim, S., Fleshman, J. W., Glenn, L. L., & Burke, R. E. (1987b). Three-dimensional architecture of dendritic trees in type-identified alpha-motoneurons. *Journal of Comparative Neurology*, *255*(1), 82–96. https://doi.org/10.1002/cne.902550107

Daou, A., Ross, M. T., Johnson, F., Hyson, R. L., & Bertram, R. (2013). Electrophysiological characterization and computational models of HVC neurons in the zebra finch. *Journal of Neurophysiology*, *110*(5), 1227–1245. https://doi.org/10.1152/jn.00162.2013

Ditz, H. M., & Nieder, A. (2015). Neurons selective to the number of visual items in the corvid songbird endbrain. *Proceedings of the National Academy of Sciences of the United States of America*, *112*(25), 7827–7832. https://doi.org/10.1073/pnas.1504245112

Dubbeldam, J. L., & Visser, A. M. (1987). The organization of the nucleus basalis-neostriatum complex of the mallard (*Anas platyrhynchos* L.) and its connections with the archistriatum and the paleostriatum complex. *Neuroscience*, *21*(2), 487–517. https://doi.org/10.1016/0306-4522(87)90137-0

Dumas, C., & Wilkie, D. M. (1995). Object permanence in ring doves (*Streptopelia risoria*). *Journal of Comparative Psychology*, *109*(2), 142–150. https://doi.org/10.1037/0735-7036.109.2.142

Düring, D. N., Dittrich, F., Rocha, M. D., Tachibana, R. O., Mori, C., Okanoya, K., Boehringer, R., Ehret, B., Grewe, B. F., Gerber, S., Ma, S., Rauch, M., Paterna, J.-C., Kasper, R., Gahr, M., & Hahnloser, R. H. R. (2020). Fast retrograde access to projection neuron circuits underlying vocal learning in songbirds. *Cell Reports*, *33*(6), 108364. https://doi.org/10.1016/j.celrep.2020.108364

Ebbesson, S. O. (1980). The parcellation theory and its relation to interspecific variability in brain organization, evolutionary and ontogenetic development, and neuronal plasticity. *Cell and Tissue Research*, *213*(2), 179–212. https://doi.org/10.1007/bf00234781

Farries, M. A. (2001). The oscine song system considered in the context of the avian brain: Lessons learned from comparative neurobiology. *Brain, Behavior and Evolution*, *58*(2), 80–100. https://doi.org/10.1159/000047263

Farries, M. A. (2004). The avian song system in comparative perspective. *Annals of the New York Academy of Sciences*, *1016*(1), 61–76. https://doi.org/10.1196/annals.1298.007

Feenders, G., Liedvogel, M., Rivas, M., Zapka, M., Horita, H., Hara, E., Wada, K., Mouritsen, H., & Jarvis, E. D. (2008). Molecular mapping of movement-associated areas in the avian brain: A motor theory for vocal learning origin. *PLoS ONE*, *3*(3), e1768. https://doi.org/10.1371/journal.pone.0001768

Fernández, M., Ahumada-Galleguillos, P., Sentis, E., Marín, G., & Mpodozis, J. (2020). Intratelencephalic projections of the avian visual dorsal ventricular ridge: Laminarly segregated, reciprocally and topographically organized. *The Journal of Comparative Neurology*, *528*(2), 321–359. https://doi.org/10.1002/cne.24757

Fernández, M., Morales, C., Durán, E., Fernández-Colleman, S., Sentis, E., Mpodozis, J., Karten, H. J., & Marín, G. J. (2020). Parallel organization of the avian sensorimotor arcopallium: Tectofugal visual pathway in the pigeon (*Columba livia*). *The Journal of Comparative Neurology*, *528*(4), 597–623. https://doi.org/10.1002/cne.24775

Fernández, M., Reyes-Pinto, R., Norambuena, C., Sentis, E., & Mpodozis, J. (2021). A canonical interlaminar circuit in the sensory dorsal ventricular ridge of birds: The anatomical organization of the trigeminal pallium. *The Journal of Comparative Neurology*, *529*(14), 3410–3428. https://doi.org/10.1002/cne.25201

Folta, K., Diekamp, B., & Güntürkün, O. (2004). Asymmetrical modes of visual bottom-up and top-down integration in the thalamic nucleus rotundus of pigeons. *Journal of Neuroscience*, *24*(43), 9475–9485. https://doi.org/10.1523/JNEUROSCI.3289-04.2004

Folta, K., Troje, N. F., & Güntürkün, O. (2007). Timing of ascending and descending visual signals predicts the response mode of single cells in the thalamic nucleus rotundus of the pigeon (*Columba livia*). *Brain Research*, *1132*(1), 100–109. https://doi.org/10.1016/j.brainres.2006.11.034

Foster, E. F., & Bottjer, S. W. (1998). Axonal connections of the High Vocal Center and surrounding cortical regions in juvenile and adult male zebra finches. *Journal of Comparative Neurology*, *397*(1), 118–138. https://doi.org/10.1002/(SICI)1096-9861(19980720)397:1⟨118::AID-CNE9⟩3.0.CO;2-3

Fujita, T., Aoki, N., Mori, C., Fujita, E., Matsushima, T., Homma, K. J., & Yamaguchi, S. (2020). The dorsal arcopallium of chicks displays the expression of orthologs of mammalian fear related serotonin receptor subfamily genes. *Scientific Reports*, *10*(1), 21183. https://doi.org/10.1038/s41598-020-78247-9

Gahr, M. (2000). Neural song control system of hummingbirds: Comparison to swifts, vocal learning (Songbirds) and nonlearning (Suboscines) passerines, and vocal learning (Budgerigars) and nonlearning (Dove, owl, gull, quail, chicken) nonpasserines. *Journal of Comparative Neurology*, *426*(2), 182–196. https://doi.org/10.1002/1096-9861(20001016)426:2⟨182::AID-CNE2⟩3.0.CO;2-M

Gao, M., Lengersdorf, D., Stüttgen, M. C., & Güntürkün, O. (2018). Nmda receptors in the avian amygdala and the premotor arcopallium mediate distinct aspects of appetitive extinction learning. *Behavioural Brain Research*, *343*, 71–82. https://doi.org/10.1016/j.bbr.2018.01.026

Güntürkün, O. (1997). Cognitive impairments after lesions of the neostriatum caudolaterale and its thalamic afferent in pigeons: Functional similarities to the mammalian prefrontal system? *Journal Für Hirnforschung*, *38*(1), 133–143.

Güntürkün, O. (2005). Avian and mammalian "prefrontal cortices": Limited degrees of freedom in the evolution of the neural mechanisms of goal-state maintenance. *Brain Research Bulletin*, *66*(4-6), 311–316. https://doi.org/10.1016/j.brainresbull.2005.02.004

Güntürkün, O. (2012). The convergent evolution of neural substrates for cognition. *Psychological Research*, *76*(2), 212–219. https://doi.org/10.1007/s00426-011-0377-9

Güntürkün, O., & Bugnyar, T. (2016). Cognition without cortex. *Trends in Cognitive Sciences*, *20*(4), 291–303. https://doi.org/10.1016/j.tics.2016.02.001

Güntürkün, O., Eugen, K. v., Packheiser, J., & Pusch, R. (2021). Avian pallial circuits and cognition: A comparison to mammals. *Current Opinion in Neurobiology*, *71*, 29–36. https://doi.org/10.1016/j.conb.2021.08.007

Güntürkün, O., Ströckens, F., Scarf, D., & Colombo, M. (2017). Apes, feathered apes, and pigeons: Differences and similarities. *Current Opinion in Behavioral Sciences*, *16*, 35–40. https://doi.org/10.1016/j.cobeha.2017.03.003

Hackett, S. J., Kimball, R. T., Reddy, S., Bowie, R. C. K., Braun, E. L., Braun, M. J., Chojnowski, J. L., Cox, W. A., Han, K.-L., Harshman, J., Huddleston, C. J., Marks, B. D., Miglia, K. J., Moore, W. S., Sheldon, F. H., Steadman, D. W., Witt, C. C., & Yuri, T. (2008). A phylogenomic study of birds reveals their evolutionary history. *Science*, *320*(5884), 1763–1768. https://doi.org/10.1126/science.1157704

Hahn, L. A., Balakhonov, D., Fongaro, E., Nieder, A., & Rose, J. (2021). Working memory capacity of crows and monkeys arises from similar neuronal computations. *eLife*, *10*, e72783. https://doi.org/10.7554/eLife.72783

Hahn, L. A., & Rose, J. (2023). Executive control of sequence behavior in pigeons involves two distinct brain regions. *eNeuro*, *10*(3), ENEURO.0296-22.2023. https://doi.org/10.1523/ENEURO.0296-22.2023

Hampton, C. M., Sakata, J. T., & Brainard, M. S. (2009). An avian basal ganglia-forebrain circuit contributes differentially to syllable versus sequence variability of adult Bengalese finch song. *Journal of Neurophysiology*, *101*(6), 3235–3245. https://doi.org/10.1152/jn.91089.2008

Helduser, S., Cheng, S., & Güntürkün, O. (2013). Identification of two forebrain structures that mediate execution of memorized sequences in the pigeon. *Journal of Neurophysiology*, *109*(4), 958–968. https://doi.org/10.1152/jn.00763.2012

Helduser, S., & Güntürkün, O. (2012). Neural substrates for serial reaction time tasks in pigeons. *Behavioural Brain Research*, *230*(1), 132–143. https://doi.org/10.1016/j.bbr.2012.02.013

Helduser, S., Westkott, M., Pawelzik, K., & Güntürkün, O. (2014). The putative pigeon homologue to song bird LMAN does not modulate behavioral variability. *Behavioural Brain Research*, *263*, 144–148. https://doi.org/10.1016/j.bbr.2014.01.019

Hellmann, B., Güntürkün, O., & Manns, M. (2004). Tectal mosaic: Organization of the descending tectal projections in comparison to the ascending tectofugal pathway in the pigeon. *Journal of Comparative Neurology*, *472*(4), 395–410. https://doi.org/10.1002/cne.20056

Herold, C., Palomero-Gallagher, N., Hellmann, B., Kröner, S., Theiss, C., Güntürkün, O., & Zilles, K. (2011). The receptor architecture of the pigeons' nidopallium caudolaterale: An avian analogue to the mammalian prefrontal cortex. *Brain Structure and Function*, *216*(3), 239–254. https://doi.org/10.1007/s00429-011-0301-5

Herold, C., Paulitschek, C., Palomero-Gallagher, N., Güntürkün, O., & Zilles, K. (2018). Transmitter receptors reveal segregation of the arcopallium/amygdala complex in pigeons (*Columba livia*). *The Journal of*

Comparative Neurology, *526*(3), 439–466. https://doi.org/10.1002/cne.24344

Heyers, D., Manns, M., Luksch, H., Güntürkün, O., & Mouritsen, H. (2008). Calcium-binding proteins label functional streams of the visual system in a songbird. *Brain Research Bulletin*, *75*(2-4), 348–355. https://doi.org/10.1016/j.brainresbull.2007.10.029

Horita, H., Kobayashi, M., Liu, W.-C., Oka, K., Jarvis, E. D., & Wada, K. (2012). Specialized motor-driven dusp1 expression in the song systems of multiple lineages of vocal learning birds. *PLoS ONE*, *7*(8), e42173. https://doi.org/10.1371/journal.pone.0042173

Husband, S. A., & Shimizu, T. (1999). Efferent projections of the ectostriatum in the pigeon (*Columba livia*). *Journal of Comparative Neurology*, *406*(3), 329–345. https://doi.org/10.1002/(SICI)1096-9861(19990412)406:3⟨329::AID-CNE3⟩3.0.CO;2-A

Jarvis, E. D. (2019). Evolution of vocal learning and spoken language. *Science*, *366*(6461), 50–54. https://doi.org/10.1126/science.aax0287

Jarvis, E. D., & Mello, C. V. (2000). Molecular mapping of brain areas involved in parrot vocal communication. *Journal of Comparative Neurology*, *419*(1), Article 1–31. https://doi.org/10.1002/(SICI)1096-9861(20000327)419:1⟨1::AID-CNE1⟩3.0.CO;2-M

Jarvis, E. D., Mirarab, S., Aberer, A. J., Li, B., Houde, P., Li, C., Ho, S. Y. W., Faircloth, B. C., Nabholz, B., Howard, J. T., Suh, A., Weber, C. C., da Fonseca, R. R., Alfaro-Núñez, A., Narula, N., Liu, L., Burt, D., Ellegren, H., Edwards, S. V., … Zhang, G. (2015). Phylogenomic analyses data of the avian phylogenomics project. *GigaScience*, *4*(1). https://doi.org/10.1186/s13742-014-0038-1

Jarvis, E. D., Ribeiro, S., Silva, M. L. D., Ventura, D., Vielliard, J., & Mello, C. V. (2000). Behaviourally driven gene expression reveals song nuclei in hummingbird brain. *Nature*, *406*(6796), 628–632. https://doi.org/10.1038/35020570

Jarvis, E. D., Scharff, C., Grossman, M. R., Ramos, J. A., & Nottebohm, F. (1998). For whom the bird sings. *Neuron*, *21*(4), 775–788. https://doi.org/10.1016/S0896-6273(00)80594-2

Jarvis, E. D., Yu, J., Rivas, M. V., Horita, H., Feenders, G., Whitney, O., Jarvis, S. C., Jarvis, E. R., Kubikova, L., Puck, A. E. P., Siang-Bakshi, C., Martin, S., McElroy, M., Hara, E., Howard, J., Pfenning, A., Mouritsen, H., Chen, C.-C., & Wada, K. (2013). Global view of the functional molecular organization of the avian cerebrum: Mirror images and functional columns. *The Journal of Comparative Neurology*, *521*(16), 3614–3665. https://doi.org/10.1002/cne.23404

Jiao, Y., Medina, L., Veenman, C. L., Toledo, C., Puelles, L., & Reiner, A. (2000). Identification of the anterior nucleus of the ansa lenticularis in birds as the homolog of the mammalian subthalamic nucleus. *The Journal of Neuroscience*, *20*(18), 6998–7010. https://doi.org/10.1523/JNEUROSCI.20-18-06998.2000

Karten, H. J. (1967). The organization of the ascending auditory pathway in the pigeon (*Columba livia*). I. Diencephalic projections of the inferior colliculus (nucleus mesencephali lateralis, pars dorsalis). *Brain Research*, *6*(3), 409–427. https://doi.org/10.1016/0006-8993(67)90055-8

Karten, H. J., & Hodos, W. (1967). *A stereotaxic atlas of the brain of the pigeon (Columba livia)*. Johns Hopkins University Press.

Karten, H. J., & Hodos, W. (1970). Telencephalic projections of the nucleus rotundus in the pigeon (*Columba livia*). *Journal of Comparative Neurology*, *140*(1), 35–51. https://doi.org/10.1002/cne.901400103

Karten, H. J., Hodos, W., Nauta, W. J., & Revzin, A. M. (1973). Neural connections of the "visual wulst" of the avian telencephalon. Experimental studies in the piegon (*Columba livia*) and owl (*Speotyto cunicularia*). *Journal of Comparative Neurology*, *150*(3), 253–278. https://doi.org/10.1002/cne.901500303

Katz, L. C., & Gurney, M. E. (1981). Auditory responses in the zebra finch's motor system for song. *Brain Research*, *221*(1), 192–197. https://doi.org/10.1016/0006-8993(81)91073-8

Kenigfest, N. B., Belekhova, M. G., & Chudinova, T. V. (2017). Distribution of calcium-binding proteins parvalbumin and calbindin in the pigeon telencephalic auditory center. *Journal of Evolutionary Biochemistry and Physiology*, *53*(2), 143–152. https://doi.org/10.1134/S1234567817020070

Kitt, C. A., & Brauth, S. E. (1982). A paleostriatal-thalamic-telencephalic path in pigeons. *Neuroscience*, *7*(11), 2735–2751. https://doi.org/10.1016/0306-4522(82)90097-5

Kobylkov, D., Musielak, I., Haase, K., Rook, N., Eugen, K. v., Dedek, K., Güntürkün, O., Mouritsen, H., & Heyers, D. (2022). Morphology of the "prefrontal" nidopallium caudolaterale in the long-distance night-migratory Eurasian blackcap (*Sylvia atricapilla*). *Neuroscience Letters*, *789*, 136869. https://doi.org/10.1016/j.neulet.2022.136869

Kobylkov, D., Schwarze, S., Michalik, B., Winklhofer, M., Mouritsen, H., & Heyers, D. (2020). A newly identified trigeminal brain pathway in a night-migratory bird could be dedicated to transmitting magnetic map information. *Proceedings of the Royal Society B: Biological Sciences*, *287*(1919), 20192788. https://doi.org/10.1098/rspb.2019.2788

Kröner, S., & Güntürkün, O. (1999). Afferent and efferent connections of the caudolateral neostriatum in the pigeon (*Columba livia*): A retro- and anterograde pathway tracing study. *Journal of Comparative Neurology*, *407*(2), 228–260.

Krützfeldt, N. O. E., & Wild, J. M. (2005). Definition and novel connections of the entopallium in the pigeon (*Columba livia*). *Journal of Comparative Neurology*, *490*(1), 40–56. https://doi.org/10.1002/cne.20627

Kuenzel, W. J., Medina, L., Csillag, A., Perkel, D. J., & Reiner, A. (2011). The avian subpallium: New insights into structural and functional subdivisions occupying the lateral subpallial wall and their embryological origins. *Brain Research*, *1424*, 67–101. https://doi.org/10.1016/j.brainres.2011.09.037

Lee, K. H., Chung, K., Chung, J. M., & Coggeshall, R. E. (1986). Correlation of cell body size, axon size, and signal conduction velocity for individually labelled dorsal root ganglion cells in the cat. *Journal of Comparative Neurology*, *243*(3), 335–346. https://doi.org/10.1002/cne.902430305

Lengersdorf, D., Pusch, R., Güntürkün, O., & Stüttgen, M. C. (2014). Neurons in the pigeon nidopallium caudolaterale signal the selection and execution of perceptual decisions. *The European Journal of Neuroscience*, *40*(9), 3316–3327. https://doi.org/10.1111/ejn.12698

Letzner, S., Simon, A., & Güntürkün, O. (2016). Connectivity and neurochemistry of the commissura anterior of the pigeon (*Columba livia*). *The Journal of Comparative Neurology*, *524*(2), 343–361. https://doi.org/10.1002/cne.23858

Leutgeb, S., Husband, S., Riters, L. V., Shimizu, T., & Bingman, V. P. (1996). Telencephalic afferents to the caudolateral neostriatum of the pigeon. *Brain Research*, *730*(1-2), 173–181. https://doi.org/10.1016/0006-8993(96)00444-1

Matsunaga, E., Kato, M., & Okanoya, K. (2008). Comparative analysis of gene expressions among avian brains: A molecular approach to the evolution of vocal learning. *Brain Research Bulletin*, *75*(2-4), 474–479. https://doi.org/10.1016/j.brainresbull.2007.10.045

Medina, L., Abellán, A., Vicario, A., & Desfilis, E. (2014). Evolutionary and developmental contributions for understanding the organization of the basal ganglia. *Brain, Behavior and Evolution*, *83*(2), 112–125. https://doi.org/10.1159/000357832

Medina, L., & Reiner, A. (1997). The efferent projections of the dorsal and ventral pallidal parts of the pigeon basal ganglia, studied with biotinylated dextran amine. *Neuroscience*, *81*(3), 773–802. https://doi.org/10.1016/S0306-4522(97)00204-2

Medina, L., & Reiner, A. (2000). Do birds possess homologues of mammalian primary visual, somatosensory and motor cortices? *Trends in Neurosciences*, *23*(1), 1–12. https://doi.org/10.1016/S0166-2236(99)01486-1

Medina, L., Veenman, C. L., & Reiner, A. (1997). Evidence for a possible avian dorsal thalamic region comparable to the mammalian ventral anterior, ventral lateral, and oral ventroposterolateral nuclei. *Journal of Comparative Neurology*, *384*(1), 86–108. https://doi.org/10.1002/(SICI)1096-9861(19970721)384:1⟨86::AID-CNE6⟩3.0.CO;2-H

Mello, C. V., Kaser, T., Buckner, A. A., Wirthlin, M., & Lovell, P. V. (2019). Molecular architecture of the zebra finch arcopallium. *The Journal of Comparative Neurology*, *527*(15), 2512–2556. https://doi.org/10.1002/cne.24688

Mello, C. V., Vates, E., Okuhata, S., & Nottebohm, F. (1998). Descending auditory pathways in the adult male zebra finch (*Taeniopygia guttata*). *Journal of Comparative Neurology*, *395*(2), 137–160. https://doi.org/10.1002/(SICI)1096-9861(19980601)395:2⟨137::AID-CNE1⟩3.0.CO;2-3

Metzger, M., Jiang, S., & Braun, K. (1998). Organization of the dorsocaudal neostriatal complex: A retrograde and anterograde tracing study in the domestic chick with special emphasis on pathways relevant to imprinting. *Journal of Comparative Neurology*, *395*(3), 380–404. https://doi.org/10.1002/(SICI)1096-9861(19980808)395:3⟨380::AID-CNE8⟩3.0.CO;2-Z

Miceli, D., Repérant, J., Villalobos, J., & Dionne, L. (1987). Extratelencephalic projections of the avian visual Wulst. A quantitative autoradiographic study in the pigeon *Columbia livia*. *Journal Für Hirnforschung*, *28*(1), 45–57. https://europepmc.org/article/med/3598175

Montagnese, C. M., Krebs, J. R., Székely, A. D., & Csillag, A. (1993). A subpopulation of large calbindin-like immunopositive neurones is present in the hippocampal formation in food-storing but not in non-storing species of bird. *Brain Research*, *614*(1-2), 291–300. https://doi.org/10.1016/0006-8993(93)91047-V

Mooney, R. (2000). Different subthreshold mechanisms underlie song selectivity in identified HVc neurons of the zebra finch. *The Journal of Neuroscience*, *20*(14), 5420–5436. https://doi.org/10.1523/JNEUROSCI.20-14-05420.2000

Mooney, R., & Prather, J. F. (2005). The HVC microcircuit: The synaptic basis for interactions between song motor and vocal plasticity pathways. *Journal of Neuroscience*, *25*(8), 1952–1964. https://doi.org/10.1523/JNEUROSCI.3726-04.2005

Moorman, S., Mello, C. V., & Bolhuis, J. J. (2011). From songs to synapses: Molecular mechanisms of birdsong memory. Molecular mechanisms of auditory learning in songbirds involve immediate early genes, including zenk and arc, the ERK/MAPK pathway and synapsins. *BioEssays: News and Reviews in Molecular, Cellular and Developmental Biology*, *33*(5), 377–385. https://doi.org/10.1002/bies.201000150

Mouritsen, H., Heyers, D., & Güntürkün, O. (2016). The neural basis of long-distance navigation in birds. *Annual Review of Physiology*, *78*, 133–154. https://doi.org/10.1146/annurev-physiol-021115-105054

Nevue, A. A., Lovell, P. V., Wirthlin, M., & Mello, C. V. (2020). Molecular specializations of deep cortical layer analogs in songbirds. *Scientific Reports*, *10*(1), 18767. https://doi.org/10.1038/s41598-020-75773-4

Nixdorf, B. E., Davis, S. S., & DeVoogd, T. J. (1989). Morphology of Golgi-impregnated neurons in hyperstriatum ventralis, pars caudalis in adult male and female canaries. *Journal of Comparative Neurology*, *284*(3), 337–349. https://doi.org/10.1002/cne.902840302

Nottebohm, F. (2005). The neural basis of birdsong. *PLoS Biology*, *3*(5), e164. https://doi.org/10.1371/journal.pbio.0030164

Nottebohm, F., Kelley, D. B., & Paton, J. A. (1982). Connections of vocal control nuclei in the canary telencephalon. *Journal of Comparative Neurology*, *207*(4), 344–357. https://doi.org/10.1002/cne.902070406

Packheiser, J., Donoso, J. R., Cheng, S., Güntürkün, O., & Pusch, R. (2021). Trial-by-trial dynamics of reward prediction error-associated signals during extinction learning and renewal. *Progress in Neurobiology*, *197*, 101901. https://doi.org/10.1016/j.pneurobio.2020.101901

Paterson, A. K., & Bottjer, S. W. (2017). Cortical inter-hemispheric circuits for multimodal vocal learning in songbirds. *The Journal of Comparative Neurology*, *525*(15), 3312–3340. https://doi.org/10.1002/cne.24280

Paton, J. A., O'Loughlin, B. E., & Nottebohm, F. (1985). Cells born in adult canary forebrain are local interneurons. *The Journal of Neuroscience*, *5*(11), 3088–3093. https://doi.org/10.1523/JNEUROSCI.05-11-03088.1985

Peng, Z., Zhang, X., Xi, C., Zeng, S., Liu, N., Zuo, M., & Zhang, X. (2012). Changes in ultra-structures and electrophysiological properties in HVC of untutored and deafened Bengalese finches relation to normally reared birds: Implications for song learning. *Brain Research Bulletin*, *89*(5-6), 211–222. https://doi.org/10.1016/j.brainresbull.2012.09.004

Petkov, C. I., & Jarvis, E. D. (2012). Birds, primates, and spoken language origins: Behavioral phenotypes and neurobiological substrates. *Frontiers in Evolutionary Neuroscience*, *4*, 12. https://doi.org/10.3389/fnevo.2012.00012

Pika, S., Sima, M. J., Blum, C. R., Herrmann, E., & Mundry, R. (2020). Ravens parallel great apes in physical and social cognitive skills. *Scientific Reports*, *10*(1), 20617. https://doi.org/10.1038/s41598-020-77060-8

Pinaud, R., Fortes, A. F., Lovell, P., & Mello, C. V. (2006). Calbindin-positive neurons reveal a sexual dimorphism within the songbird analogue of the mammalian auditory cortex. *Journal of Neurobiology*, *66*(2), 182–195. https://doi.org/10.1002/neu.20211

Prior, H., Wiltschko, R., Stapput, K., Güntürkün, O., & Wiltschko, W. (2004). Visual lateralization and homing in pigeons. *Behavioural Brain Research*, *154*(2), 301–310. https://doi.org/10.1016/j.bbr.2004.02.018

Pusch, R., Clark, W., Rose, J., & Güntürkün, O. (2023). Visual categories and concepts in the avian brain. *Animal Cognition*, *26*(1), 153–173. https://doi.org/10.1007/s10071-022-01711-8

Redies, C., Medina, L., & Puelles, L. (2001). Cadherin expression by embryonic divisions and derived gray matter structures in the telencephalon of the chicken. *Journal of Comparative Neurology*, *438*(3), 253–285.

Reiner, A. (2002). Functional circuitry of the avian basal ganglia: Implications for basal ganglia organization in stem amniotes. *Brain Research Bulletin*, *57*(3-4), 513–528. https://doi.org/10.1016/S0361-9230(01)00667-0

Reiner, A., Laverghetta, A. V., Meade, C. A., Cuthbertson, S. L., & Bottjer, S. W. (2004). An immunohistochemical and pathway tracing study of the striatopallidal organization of area X in the male zebra finch. *Journal of Comparative Neurology*, *469*(2), 239–261. https://doi.org/10.1002/cne.11012

Roberts, T. F., Gobes, S. M. H., Murugan, M., Ölveczky, B. P., & Mooney, R. (2012). Motor circuits are required to encode a sensory model for imitative learning. *Nature Neuroscience*, *15*(10), 1454–1459. https://doi.org/10.1038/nn.3206

Rook, N., Letzner, S., Packheiser, J., Güntürkün, O., & Beste, C. (2020). Immediate early gene fingerprints of multi-component behaviour. *Scientific Reports*, *10*(1), 384. https://doi.org/10.1038/s41598-019-56998-4

Rook, N., Stacho, M., Schwarz, A., Bingman, V. P., & Güntürkün, O. (2023). Neuronal circuits within the homing pigeon hippocampal formation. *The Journal of Comparative Neurology*, *531*(7), 790–813. https://doi.org/10.1002/cne.25462

Rook, N., Tuff, J. M., Isparta, S., Masseck, O. A., Herlitze, S., Güntürkün, O., & Pusch, R. (2021). Aav1 is the optimal viral vector for optogenetic experiments in pigeons (Columba livia). *Communications Biology*, *4*(1), 100. https://doi.org/10.1038/s42003-020-01595-9

Rook, N., Tuff, J. M., Packheiser, J., Güntürkün, O., & Beste, C. (2021). A hierarchical processing unit for multi-component behavior in the avian brain. *iScience*, *24*(10), 103195. https://doi.org/10.1016/j.isci.2021.103195

Rose, J., Schiffer, A.-M., & Güntürkün, O. (2013). Striatal dopamine D1 receptors are involved in the dissociation of learning based on reward-magnitude. *Neuroscience*, *230*, 132–138. https://doi.org/10.1016/j.neuroscience.2012.10.064

Scarf, D., Boy, K., Uber Reinert, A., Devine, J., Güntürkün, O., & Colombo, M. (2016). Orthographic processing in pigeons (*Columba livia*). *Proceedings of the National Academy of Sciences of the United States of America*, *113*(40), 11272–11276. https://doi.org/10.1073/pnas.1607870113

Scarf, D., Hayne, H., & Colombo, M. (2011). Pigeons on par with primates in numerical competence. *Science*, *334*(6063), 1664. https://doi.org/10.1126/science.1213357

Shaevitz, S. S., & Theunissen, F. E. (2007). Functional connectivity between auditory areas field L and CLM and song system nucleus HVC in anesthetized zebra finches. *Journal of Neurophysiology*, *98*(5), 2747–2764. https://doi.org/10.1152/jn.00294.2007

Shanahan, M., Bingman, V. P., Shimizu, T., Wild, J. M., & Güntürkün, O. (2013). Large-scale network organization in the avian forebrain: A connectivity matrix and theoretical analysis. *Frontiers in Computational Neuroscience*, *7*, 89. https://doi.org/10.3389/fncom.2013.00089

Shimizu, T., Cox, K., & Karten, H. J. (1995). Intratelencephalic projections of the visual wulst in pigeons (*Columba livia*). *Journal of Comparative Neurology*, *359*(4), 551–572. https://doi.org/10.1002/cne.903590404

Stacho, M., Herold, C., Rook, N., Wagner, H., Axer, M., Amunts, K., & Güntürkün, O. (2020). A cortex-like canonical circuit in the avian forebrain. *Science*, *369*(6511), eabc5534. https://doi.org/10.1126/science.abc5534

Ströckens, F., Neves, K., Kirchem, S., Schwab, C., Herculano-Houzel, S., & Güntürkün, O. (2022). High associative neuron numbers could drive cognitive performance in corvid species. *The Journal of Comparative Neurology*, *530*(10), 1588–1605. https://doi.org/10.1002/cne.25298

Trusel, M., Alam, D., & Roberts, T. F. (2022). Synaptic connectivity of afferent inputs onto projection neurons in the songbird HVC. bioRxiv. https://doi.org/10.1101/2022.11.08.515692

Vates, G. E., Broome, B. M., Mello, C. V., & Nottebohm, F. (1996). Auditory pathways of caudal telencephalon and their relation to the song system of adult male zebra finches (*Taenopygia guttata*). *Journal of Comparative Neurology*, *366*(4), 613–642. https://doi.org/10.1002/(SICI)1096-9861(19960318)366:4⟨613::AID-CNE5⟩3.0.CO;2-7

Veenman, C. L., Wild, J. M., & Reiner, A. (1995). Organization of the avian "corticostriatal" projection system: A retrograde and anterograde pathway tracing study in pigeons. *Journal of Comparative Neurology*, *354*(1), 87–126. https://doi.org/10.1002/cne.903540108

von Eugen, K., Tabrik, S., Güntürkün, O., & Ströckens, F. (2020). A comparative analysis of the dopaminergic innervation of the executive caudal nidopallium in pigeon, chicken, zebra finch, and carrion crow. *The Journal of Comparative Neurology*, *528*(17), 2929–2955. https://doi.org/10.1002/cne.24878

Wagner, H., Güntürkün, O., & Nieder, B. (2003). Anatomical markers for the subdivisions of the barn owl's inferior-collicular complex and adjacent peri- and subventricular structures. *Journal of Comparative Neurology*, *465*(1), 145–159. https://doi.org/10.1002/cne.10826

Waldmann, C., & Güntürkün, O. (1993). The dopaminergic innervation of the pigeon caudolateral forebrain: Immunocytochemical evidence for a 'prefrontal cortex' in birds? *Brain Research*, *600*(2), 225–234. https://doi.org/10.1016/0006-8993(93)91377-5

Wang, Y., Brzozowska-Prechtl, A., & Karten, H. J. (2010). Laminar and columnar auditory cortex in avian brain. *Proceedings of the National Academy of Sciences of the United States of America*, *107*(28), 12676–12681. https://doi.org/10.1073/pnas.1006645107

Watanabe, S. (2001). Effects of lobus parolfactorius lesions on repeated acquisition of spatial discrimination in pigeons. *Brain, Behavior and Evolution*, *58*(6), 333–342. https://doi.org/10.1159/000057574

Wild, J. M. (1987). Thalamic projections to the paleostriatum and neostriatum in the pigeon (*Columba livia*). *Neuroscience*, *20*(1), 305–327. https://doi.org/10.1016/0306-4522(87)90022-4

Wild, J. M. (1992). Direct and indirect "cortico"-rubral and rubro-cerebellar cortical projections in the pigeon. *Journal of Comparative Neurology*, *326*(4), 623–636. https://doi.org/10.1002/cne.903260409

Wild, J. M., Arends, J. J., & Zeigler, H. P. (1985). Telencephalic connections of the trigeminal system in the pigeon (*Columba livia*): A trigeminal sensorimotor circuit. *Journal of Comparative Neurology*, *234*(4), 441–464. https://doi.org/10.1002/cne.902340404

Wild, J. M., & Farabaugh, S. M. (1996). Organization of afferent and efferent projections of the nucleus basalis prosencephali in a passerine, *Taeniopygia guttata*. *Journal of Comparative Neurology*, *365*(2), 306–328. https://doi.org/10.1002/(SICI)1096-9861(19960205)365:2⟨306::AID-CNE8⟩3.0.CO;2-9

Wild, J. M., Karten, H. J., & Frost, B. J. (1993). Connections of the auditory forebrain in the pigeon (*Columba livia*). *Journal of Comparative Neurology*, *337*(1), 32–62. https://doi.org/10.1002/cne.903370103

Wild, J. M., Li, D., & Eagleton, C. (1997). Projections of the dorsomedial nucleus of the intercollicular complex (DM) in relation to respiratory-vocal nuclei in the brainstem of pigeon (*Columba livia*) and zebra finch (*Taeniopygia guttata*). *Journal of Comparative Neurology*, *377*(3), 392–413. https://doi.org/10.1002/(SICI)1096-9861(19970120)377:3⟨392::AID-CNE7⟩3.0.CO;2-Y

Wild, J. M., & Williams, M. N. (2000). Rostral Wulst in passerine birds. I. Origin, course, and terminations of an avian pyramidal tract. *Journal of Comparative Neurology*, *416*(4), 429–450. https://doi.org/10.1002/(SICI)1096-9861(20000124)416:4⟨429::AID-CNE2⟩3.0.CO;2-X

Wild, J. M., Williams, M. N., Howie, G. J., & Mooney, R. (2005). Calcium-binding proteins define interneurons in HVC of the zebra finch (*Taeniopygia guttata*). *Journal of Comparative Neurology*, *483*(1), 76–90. https://doi.org/10.1002/cne.20403

Xiao, L., Chattree, G., Oscos, F. G., Cao, M., Wanat, M. J., & Roberts, T. F. (2018). A basal ganglia circuit sufficient to guide birdsong learning. *Neuron*, *98*(1), 208.e5–221.e5. https://doi.org/10.1016/j.neuron.2018.02.020

Xiao, L., Merullo, D. P., Koch, T. M. I., Cao, M., Co, M., Kulkarni, A., Konopka, G., & Roberts, T. F. (2021). Expression of FoxP2 in the basal ganglia regulates vocal motor sequences in the adult songbird. *Nature Communications*, *12*(1), 2617. https://doi.org/10.1038/s41467-021-22918-2

Xiao, L., & Roberts, T. F. (2021). What is the role of thalamostriatal circuits in learning vocal sequences? *Frontiers in Neural Circuits*, *15*, 724858. https://doi.org/10.3389/fncir.2021.724858

Xiao, Q., & Güntürkün, O. (2018). Asymmetrical commissural control of the subdominant hemisphere in pigeons. *Cell Reports*, *25*(5), 1171.e3–1180.e3. https://doi.org/10.1016/j.celrep.2018.10.011

Yamamoto, K., & Reiner, A. (2005). Distribution of the limbic system-associated membrane protein (LAMP) in pigeon forebrain and midbrain. *Journal of Comparative Neurology*, *486*(3), 221–242. https://doi.org/10.1002/cne.20562

Yamamoto, K., Sun, Z., Wang, H. B., & Reiner, A. (2005). Subpallial amygdala and nucleus taeniae in birds resemble extended amygdala and medial amygdala in mammals in their expression of markers of regional identity. *Brain Research Bulletin*, *66*(4-6), 341–347. https://doi.org/10.1016/j.brainresbull.2005.02.016

Yin, H. H. (2010). The sensorimotor striatum is necessary for serial order learning. *Journal of Neuroscience*, *30*(44), 14719–14723. https://doi.org/10.1523/JNEUROSCI.3989-10.2010

Zeier, H., & Karten, H. J. (1971). The archistriatum of the pigeon: Organization of afferent and efferent connections. *Brain Research*, *31*(2), 313–326. https://doi.org/10.1016/0006-8993(71)90185-5

Zemel, B. M., Nevue, A. A., Tavares, L. E., Dagostin, A., Lovell, P. V., Jin, D. Z., Mello, C. V., & Gersdorff, H. V. (2022). Cortical Betz cells analogue in songbirds utilizes Kv3.1 to generate ultranarrow spikes. bioRxiv. https://doi.org/10.1101/2022.08.22.504741

How to cite this article: Steinemer, A., Simon, A., Güntürkün, O., & Rook, N. (2024). Parallel executive pallio-motor loops in the pigeon brain. *Journal of Comparative Neurology*, *532*, e25611. https://doi.org/10.1002/cne.25611